










ARTICLE

Activated PI3K δ signals compromise plasma cell survival via limiting autophagy and increasing ER stress

Fahd Al Qureshah^{1,2,3} , Sara Sagadiev¹ , Christopher D. Thouvenel¹ , Shuozhi Liu¹ , Zhaolin Hua⁴ , Baidong Hou⁴ , Mridu Acharya¹ , Richard G. James^{1,5,6} , and David J. Rawlings^{1,2,5} 

While phosphatidylinositide 3-kinase delta (PI3K δ) plays a critical role in humoral immunity, the requirement for PI3K δ signaling in plasma cells remains poorly understood. Here, we used a conditional mouse model of activated PI3K δ syndrome (APDS), to interrogate the function of PI3K δ in plasma cell biology. Mice expressing a PIK3CD gain-of-function mutation (aPIK3CD) in B cells generated increased numbers of memory B cells and mounted an enhanced secondary response but exhibited a rapid decay of antibody levels over time. Consistent with these findings, aPIK3CD expression markedly impaired plasma cell generation, and expression of aPIK3CD intrinsically in plasma cells was sufficient to diminish humoral responses. Mechanistically, aPIK3CD disrupted ER proteostasis and autophagy, which led to increased plasma cell death. Notably, this defect was driven primarily by elevated mTORC1 signaling and modulated by treatment with PI3K δ -specific inhibitors. Our findings establish an essential role for PI3K δ in plasma cell homeostasis and suggest that modulating PI3K δ activity may be useful for promoting and/or thwarting specific immune responses.

Introduction

Antibodies produced by plasma B cells (PCs) are a hallmark of humoral immunity and provide protection against infection and reinfection. Depending upon the context of antigen encounter, activated B cells proliferate and differentiate into antibody-secreting cells (ASCs) or memory B cells (MBCs). Plasmablasts are short-lived ASCs that are generated early during the immune response (Nutt et al., 2015). In contrast, long-lived PCs are predominately derived from germinal centers (GCs) and home to, and preferentially reside in, the bone marrow (BM) to sustain high titers of protective antibodies for decades. In parallel, GCs also produce MBCs that are retained in lymphoid tissues and poised to rapidly differentiate into short- and long-lived PCs following reexposure to antigen (Kurosaki et al., 2015). Thus, understanding key factors that control the differentiation, function, and survival of PCs is critical for development of new therapeutic approaches to either enhance humoral immunity to vaccination or to attenuate pathogenic humoral responses in autoimmune or malignant diseases.

Differentiation of B cells into PCs requires a coordinated genetic reprogramming via modulation of key transcription

factors, including silencing of Pax5, Bach2, and Bcl6 and activation of IRF4 and Blimp-1 (Nutt et al., 2015). As terminally differentiated B cells, PCs exhibit an exceptional capacity to produce and secrete high levels of antibodies. To accommodate these sustained functional activities, the PC differentiation program entails unique mechanisms to permit enhanced protein accumulation and ER stress while maintaining survival. First, PCs display a distinctive morphology with an expanded cytoplasm and a tightly arranged cisternae of rough ER. Second, PCs continuously activate the unfolded protein response (UPR), a homeostatic, adaptive signaling program that promotes the recovery of ER proteostasis and thereby permits cell survival in the setting of these major metabolic challenges (Bettigole and Glimcher, 2015). Further, autophagy counterbalances ER stress by eliminating excess ER while supplying metabolic substrates to maintain PC viability (Pengo et al., 2013).

Phosphatidylinositide 3-kinase (PI3K) signaling plays a critical role in the activation and function of nearly all cell lineages. Among PI3K family proteins, p110 δ , the catalytic subunit of PI3K δ , is expressed predominantly in lymphocytes and is

¹Center for Immunity and Immunotherapy, Seattle Children's Research Institute, Seattle, WA; ²Departments of Immunology, University of Washington, Seattle, WA; ³King Abdulaziz City for Science and Technology, Riyadh, Saudi Arabia; ⁴Institute of Biophysics, Chinese Academy of Sciences, Beijing, China; ⁵Departments of Pediatrics, University of Washington, Seattle, WA; ⁶Departments of Pharmacology, University of Washington, Seattle, WA.

Correspondence to David J. Rawlings: drawling@u.washington.edu.

© 2021 Al Qureshah et al. This article is distributed under the terms of an Attribution–Noncommercial–Share Alike–No Mirror Sites license for the first six months after the publication date (see <http://www.rupress.org/terms/>). After six months it is available under a Creative Commons License (Attribution–Noncommercial–Share Alike 4.0 International license, as described at <https://creativecommons.org/licenses/by-nc-sa/4.0/>).

essential for humoral immune responses (Lucas et al., 2016). p110 δ is required for antigen receptor-driven activation and differentiation of B and T cells (Preite et al., 2019). Both loss- and gain-of-function mutations in the gene encoding p110 δ (*PIK3CD*) lead to human immune dysregulation (Fruman et al., 2017; Lucas et al., 2016), albeit through different mechanisms, events that have been partially elucidated in mouse models. Mice expressing catalytically inactive (or lacking) p110 δ in T cells exhibit impaired humoral responses due to defective T follicular helper cell formation (Okkenhaug et al., 2002; Rolf et al., 2010). Conversely, B cell-specific activation of PI3K signaling using *Foxo1* or *Pten* knockout mice results in loss of B cell class-switch recombination (CSR) and affinity maturation in response to T cell-dependent (TD) immunizations (Suzuki et al., 2003; Omori et al., 2006; Dengler et al., 2008; Sander et al., 2015; Dominguez-Sola et al., 2015). Further, mice expressing activating mutations in *PIK3CD*, referred to hereafter as activated (a) *PIK3CD* mice, display a broad range of alterations in immune function, including decreased antigen-specific class-switched antibodies (Wray-Dutra et al., 2018; Preite et al., 2018; Avery et al., 2018; Stark et al., 2018). a*PIK3CD* mice mimic the most common heterozygous mutation present in the human immunodeficiency disease, activated PI3K δ syndrome (APDS; Angulo et al., 2013; Crank et al., 2014; Lucas et al., 2014; Coulter et al., 2017). Both global and B cell-intrinsic a*PIK3CD* mice (Wray-Dutra et al., 2018) exhibit a reduction in class-switched antibodies, mirroring the reduced IgG levels and proportion of MBCs in APDS subjects. However, while previous work has suggested these deficits primarily reflect defective CSR (Preite et al., 2018; Avery et al., 2018), the specific role for a*PIK3CD* signaling in differentiation and function of activated, mature B cells has not been determined.

Herein, we investigated how B cell-intrinsic a*PIK3CD* signals specifically impact MBC and PC biology. Surprisingly, we found a*PIK3CD* increased the generation of antigen-specific MBCs but altered the antibody response kinetics following secondary antigen challenge. Strikingly, our detailed investigation showed that a*PIK3CD* markedly limited PC generation and survival. Elevated PI3K δ activity led to increased ER stress and impaired autophagy in PCs, thereby compromising PC survival. Together, our findings demonstrate that modulation of PI3K δ signaling is essential for PC development via regulating the UPR and autophagy via the mTORC1 pathway to mitigate ER stress and thereby ensure PC survival.

Results

Activated PI3K δ enhances antigen-specific MBC formation

To investigate the impact of activated PI3K δ signaling in MBC function, we first crossed mice harboring an endogenous *loxP*-flanked allele encoding the murine equivalent of the most common gain-of-function mutation of *PIK3CD* in APDS patients (E1021K [E1020K in mice]) with CD21-Cre mice (*Cd21^{Cre/+} Pik3cd^{E1020K/+}*) to express the variant in mature B cells (hereafter CD21-a*PIK3CD*; Wray-Dutra et al., 2018). To assess the TD memory response, we immunized CD21-a*PIK3CD* and CD21-WT littermate controls with virus-like particles (VLPs) containing a TLR ligand

(VLP-ssRNA; Hou et al., 2011). 90 d after immunization, VLP-specific MBCs were isolated using magnetic bead-based enrichment as previously described (Liao et al., 2017; Krishnamurthy et al., 2016; Taylor et al., 2012). VLP⁺ B cells were gated within B220⁺ and B220^{lo} CD138⁺, and VLP-specific MBCs were identified as CD138⁻GL7⁻CD38⁺ (Fig. S1 A). Based on this gating strategy, CD21-a*PIK3CD* mice had increased numbers of VLP-specific IgM⁺ MBCs and similar numbers of switched (IgM⁻IgD⁻) MBCs compared with control mice (Fig. 1, A–C; and Fig. S1 B). To further define cells with a memory phenotype, we assessed VLP⁺CD73⁺CD80⁺ MBCs (Fig. S1 C). CD21-a*PIK3CD* mice exhibited significantly increased numbers of both IgM⁺ and switched VLP⁺CD73⁺CD80⁺ MBCs compared with controls (Fig. 1 C).

To assess the effect of activated PI3K δ on MBC development in the same inflammatory environment, we used chimeras containing cells with both genotypes. To minimize confounding effects of PI3K on development, we induced a*PIK3CD* in GC B cells by crossing *Pik3cd^{E1020K/+}* with activation-induced cytidine deaminase (AID)-Cre (hereafter AID-a*PIK3CD*). Mixed BM chimeras were generated by transferring a 1:1 mixture of CD45.2 AID-a*PIK3CD* and CD45.1/2 AID-WT cell or CD45.2 AID-WT and CD45.1/2 AID-WT cells, respectively, into lethally irradiated CD45.1 WT hosts. Reconstituted mice were immunized with VLP-ssRNA and analyzed 90 d after immunization. Consistent with the proportional input populations, all chimeras exhibited a 1:1 ratio of CD45.2 versus CD45.1/2 cells within the IgD⁺ naive/MBC compartment. In contrast, AID-a*PIK3CD*:AID-WT recipients exhibited a ~4:1 skewing for switched MBCs compared with 1:1 ratio for AID-WT:AID-WT controls (Fig. 1 D). Together, these findings demonstrate that activated PI3K δ signaling promotes the generation of both IgM⁺ and switched MBCs and raised the question of how CD21-a*PIK3CD* mice would respond to a secondary challenge.

a*PIK3CD* mice exhibit altered MBC-dependent antibody responses

To understand whether a*PIK3CD* could impact the kinetics of the humoral response following secondary challenge, we immunized CD21-a*PIK3CD* and CD21-WT mice with VLP-ssRNA. On day 90 after immunization, the mice were left unchallenged or rechallenged with RNA-free VLP (Fig. 1 E), an immunogen that induces class-switched antibodies only in the setting of primary immunization with VLP-ssRNA. As predicted (Wray-Dutra et al., 2018), IgG2c VLP-specific antibodies were reduced in CD21-a*PIK3CD* primary-only recipients compared with controls (Fig. 1 F). Surprisingly, within 3 d of rechallenge, VLP-specific IgG2c levels in CD21-a*PIK3CD* mice increased over primary-only levels, while titers in WT mice remained unchanged (Fig. 1 F, far left). By day 5, CD21-a*PIK3CD* mice exhibited IgG2c levels that exceeded those in WT mice (Fig. 1 F) and remained above WT counterparts at 21 d after rechallenge (Fig. 1 F, middle). In contrast, at later time points, CD21-a*PIK3CD* mice exhibited a decline in IgG2c, reaching levels equivalent to controls by day 90 (Fig. 1 F, right).

To gain insight into these unexpected kinetics, we performed VLP-specific ELISPOT assays to quantify ASC number and

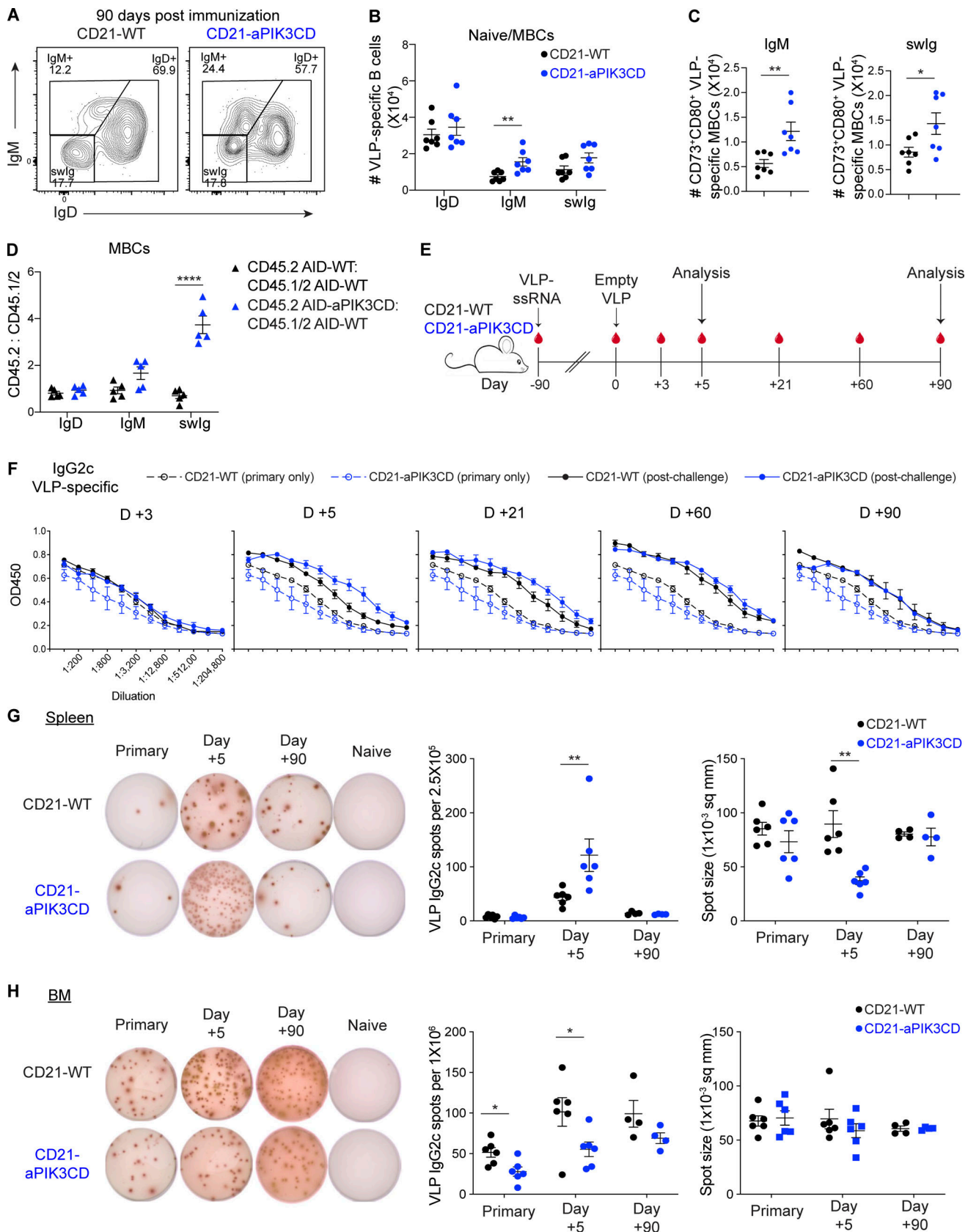


Figure 1. **Enhanced MBC numbers and altered rechallenge response in CD21-aPIK3CD mice.** (A) Flow cytometry analysis of enriched VLP-specific MBCs isotypes: IgM, IgD, and switched (swlg; gated within GL7⁻CD38⁺; see Fig. S1) at 90 d after immunization with VLP-ssRNA in CD21-WT and CD21-aPIK3CD mice. (B) Number of VLP-specific IgM, IgD, and switched MBCs 90 d after immunization. (C) Number of CD73⁺ CD80⁺ VLP-specific IgM and switched MBCs at 90 d

after immunization. **(D)** Ratio of CD45.2/CD45.1/2 VLP-specific, IgM, IgD, and switched MBCs in mixed BM chimeras of generated using CD45.2 AID-WT: CD45.1/2 AID-WT (1:1) or CD45.2 AID-aPIK3CD/CD45.1/2 AID-WT (1:1), respectively, at 90 d after immunization with VLP-ssRNA. **(E)** Schematic diagram of rechallenge experiments. CD21-WT and CD21-aPIK3CD mice were immunized intraperitoneally with VLP-ssRNA. 90 d later, mice were rechallenged with an empty (RNA-free) VLP (designated after challenge) or left unchallenged (designated primary only). Mice were bled at indicated time points, and specific cohorts were sacrificed for tissue analysis at 5 or 90 d after rechallenge. **(F)** Dilution curves of VLP-specific IgG2c prechallenge and at day (D) 3, 5, 21, 60, or 90 after challenge as measured by ELISA. **(G)** Representative images of VLP-specific IgG2c ELISPOT analysis using splenic cells from primary only or splenic cells collected at day 5 or 90 after challenge from CD21-WT or CD21-aPIK3CD mice (left). Number of VLP-specific IgG2c spots per 2.5×10^5 cells (middle) and the average spots size (right). **(H)** Representative images of VLP-specific IgG2c ELISPOTs using BM cells from primary only or BM cells collected at day 5 or 90 after challenge from CD21-WT or CD21-aPIK3CD mice (left), number of VLP-specific IgG2c spots per 10^6 (middle), and average spot size (right). Data are combined from two independent experiments (A–C: $n = 7$; D: $n = 5$; F–H: $n = 4$ –6). ELISPOT images (G and H) are representative of two independent experiments. Significance determined by two-way ANOVA multiple comparison (B, D, G, and H) or unpaired Student's *t* test (C). *, $P < 0.05$; **, $P < 0.01$; ****, $P < 0.0001$. Graphs depict mean \pm SEM.

productivity. Consistent with serum antibody levels, splenic populations in CD21-aPIK3CD mice contained a higher number of spots at day 5 after rechallenge (Fig. 1 G, middle). In contrast, the spot size of these splenic ASCs was significantly smaller than in controls (Fig. 1 G, left and right). Notably, consistent with the rapid induction of splenic ASC after rechallenge (as well as the reduced initial primary antibody response), ASC numbers in the BM of CD21-aPIK3CD were lower than in controls at day 5. Further, at 90 d after rechallenge (Fig. 1, G and H), a time point where long-lived PCs (LLPCs) are predicted to populate the BM, spot numbers remained lower in CD21-aPIK3CD mice, findings consistent with a more rapid decay of antibody levels. We also evaluated VLP-specific IgM response upon rechallenge. VLP-specific IgM was not detectable before rechallenge in either genotype. However, by day 5, CD21-aPIK3CD mice exhibited a trend for increased IgM (Fig. S1 D). Despite this increase, and in contrast to control mice, VLP-specific IgM ASCs remained undetectable in the spleen or BM (Fig. S1 E). Together, these data show that CD21-aPIK3CD mice exhibit an increased ASC response upon antigen rechallenge but are not able to sustain antibody production over time, suggesting that inappropriate PI3K δ signaling disrupts PC longevity and/or function but does not alter MBC formation.

Activated PI3K δ impairs PC development in vivo and in vitro

We next interrogated the effect of activated PI3K δ on PC formation during a primary immune response in vivo. CD21-aPIK3CD and CD21-WT mice were immunized with VLP-ssRNA. At day 14 after immunization, VLP-specific CD138⁺ PCs were markedly reduced in CD21-aPIK3CD mice compared with controls (Fig. 2 A). Moreover, CD21-aPIK3CD exhibited significantly reduced VLP-specific IgG and IgG2c PCs in spleen and BM, as measured by intracellular flow cytometry (Fig. 2 B) and ELISPOT (Fig. 2 D). In contrast, IgM PCs were present in similar numbers in CD21-aPIK3CD and controls (Fig. 2, C and D). The decrease in PC numbers CD21-aPIK3CD mice was not secondary to a reduced GC response. Total GC B cells were increased (Fig. S2 A), and the absolute number of VLP-specific and Ig2C⁺ VLP-specific GC B cells in CD21-aPIK3CD mice was similar to controls (Fig. S2, B and C).

Next, to evaluate the potential impact of aPIK3CD on PC generation in a competitive environment, we established BM chimera mice as in Fig. 1 D, immunized these recipients with VLP-ssRNA, and analyzed them at 14 d after immunization (Fig.

S3 A). VLP-specific aPIK3CD GC B cells outcompeted WT GC cells, resulting in ~ 2.5 :1 skewing as compared controls (Fig. S3, B and C). Similar to what we observed previously (Wray-Dutra et al., 2018), AID-aPIK3CD GC B cells were enriched for cells with a light zone (LZ) phenotype (Fig. S3 D). Strikingly, despite the preferential expansion of aPIK3CD cells within GC, the VLP-specific PC-to-GC B cell ratio was significantly lower AID-aPIK3CD chimera mice (Fig. 2 E and Fig. S3 B), suggesting counterselection of antigen-specific PCs. These findings demonstrate that while aPIK3CD increased the expansion and selection of antigen-specific GC B cells, aPIK3CD impairs the generation or survival of PCs.

To begin to determine how aPIK3CD modulates PC biology, we next used an in vitro culture system capable of modeling differentiation of mouse naive B cells into PCs (Nojima et al., 2011). In this system, CD21-aPIK3CD or CD21-WT B cells were cocultured with CD40LB stromal cells coexpressing membrane-bound CD40L and the secreted prosurvival cytokine B cell activating factor. To generate plasmablasts, cultures were costimulated with R848 and IL-21. Although CD21-aPIK3CD B cells cultures generated slightly but significantly more CD138⁺ plasmablasts at day 4, CD21-aPIK3CD B cell cultures generated significantly fewer CD138⁺ plasmablasts at days 6 and 7 (Fig. 2 F and Fig. S3 E). Similar data demonstrating a reduction in plasmablasts in CD21-aPIK3CD B cell cultures were observed with other relevant activating stimuli, including IL-4 + IL-21, LPS + IL-4, and LPS + IL-21 (Fig. S3 F). Together, these data demonstrate that hyperactive PI3K δ signaling inhibits PC formation.

Previous studies attributed the impaired humoral response caused by hyperactive PI3K δ to a CSR defect (Avery et al., 2018; Preite et al., 2018), mainly driven by reduced AID expression (Avery et al., 2018). Our mouse model represents a robust tool to examine the effect of aPIK3CD at specific B cell developmental stages. We previously showed that mice expressing aPIK3CD under the control of *Aicda* locus, in which B cells become overactive following AID expression, still exhibit diminished production of VLP-specific class-switched antibodies despite normal GC reactions (Wray-Dutra et al., 2018). To evaluate whether aPIK3CD signaling impacts affinity maturation, we immunized AID-aPIK3CD and controls with NP-CGG in alum and measured the titers of total NP30-binding and high-affinity NP4-binding antibodies at day 14 by ELISA. We found that both NP4- and NP30-specific IgG1 levels in the serum were significantly lower (Fig. S3 G) in AID-aPIK3CD mice. However, there

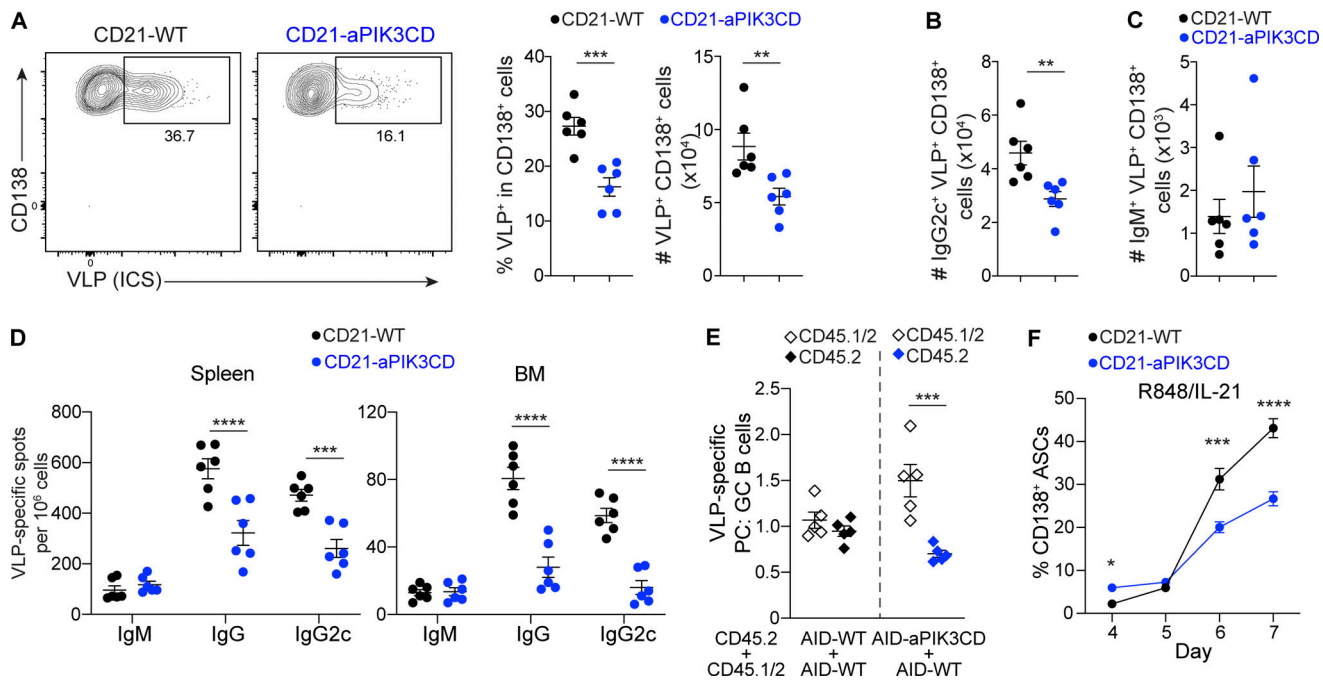


Figure 2. B cell-intrinsic expression of activated PI3K δ impairs PC generation. (A) Flow cytometry analysis of intracellular VLP staining in splenic CD138⁺ PCs (left) and frequency and absolute number of VLP-specific PCs (right) in CD21-WT or CD21-aPIK3CD mice at day 14 after immunization with VLP-ssRNA. (B and C) Quantification of IgG2c and IgM VLP-specific PCs as measured by flow cytometry. (D) Number of VLP-specific IgM, IgG, and IgG2c PCs in the spleen (left) and BM (right) determined by ELISPOT assay. (E) The ratio of VLP-specific PC to VLP-specific GC B cells at day 14 after immunization with VLP-ssRNA in mixed BM chimera recipients (previously transplanted with 1:1 ratio of CD45.2 AID-WT/CD45.1/2 AID-WT or CD45.2 AID-aPIK3CD/CD45.1/2 AID-WT BM cells, respectively). (F) Percentage of CD138⁺ ASCs generated over time from CD21-WT versus CD21-aPIK3CD B cells cultured in vitro on 40LB stroma plus R848 and IL-21. Data are combined from two (A–D: $n = 6$; E: $n = 5$) or three (F: $n = 3$ –5 at each time point) independent experiments. Significance determined by unpaired Student's t test. **, $P < 0.01$; ***, $P < 0.001$; ****, $P < 0.0001$. Graphs depict mean \pm SEM.

was no difference in the ratio of NP4 to NP30 IgG1, which suggested that aPIK3CD does not alter affinity maturation, consistent with previously published studies (Preite et al., 2018; Avery et al., 2018). Next, we assessed the humoral response using the $\text{C}\gamma 1$ -Cre strain, where aPIK3CD is expressed subsequent to CSR, leading to IgG1 expression. $\text{C}\gamma 1$ -aPIK3CD mice exhibited a significant decrease in NP4- and NP30-specific serum IgG1 levels at 14 d after immunization with NP-CGG, again without differences in the ratio of NP4 to NP30 IgG1 (Fig. S3 H). Together, these data demonstrate that aPIK3CD expression leads to a defect in the magnitude of class-switched, antigen-specific antibody responses via a mechanism independent of AID expression and CSR.

PC-intrinsic aPIK3CD expression is sufficient to alter humoral responses

Based on the above findings, we next performed studies to directly determine whether aPIK3CD exerts a PC-intrinsic impact on PC survival or function. We crossed $\text{Pik3cd}^{\text{E1020K/+}}$ mice with Blimp1-Cre strain (hereafter, Blimp1-aPIK3CD). To track Blimp1-expressing cells in this model, we also crossed Blimp1-Cre with a loxP-flanked stop cassette EYFP strain controlled by the constitutively expressed Rosa26 promoter. Following immunization with VLP-ssRNA, 80–85% of PCs expressed YFP, while less than 8% of naive B cells, T cells, GC B cells, and non-B/T cells expressed YFP (Fig. S4 A). Thus, the Blimp1-aPIK3CD

mice largely represent a PC-intrinsic model of activated PI3K δ .

To evaluate the humoral response in these mice, Blimp1-aPIK3CD and control mice were immunized with VLP-ssRNA and analyzed 14 d after immunization. Consistent with near absence of aPIK3CD expression before PC commitment, we observed no difference in GC events, including the number and frequency of total and VLP-specific GC B cells, switching to IgG2c, or dark zone (DZ)/LZ polarization (Fig. S4, B–E). However, the proportion and number of VLP-specific PCs in Blimp1-aPIK3CD mice was significantly reduced compared with controls (Fig. 3 A). Moreover, the number of VLP-specific IgM⁺, IgG⁺, and IgG2c⁺ PCs were significantly decreased in Blimp1-aPIK3CD compared with controls, as measured by flow cytometry and ELISPOT (Fig. 3, B–D). Finally, serum levels of VLP-specific IgM, IgG, and IgG2c antibodies were significantly diminished in Blimp1-aPIK3CD (Fig. 3 E). Together, these data demonstrate that hyperactive PI3K δ signaling prevents maturation of PCs.

aPIK3CD deregulates the PC gene expression program

To explore the cellular mechanisms underlying the humoral defect observed in aPIK3CD mice, we performed RNA sequencing (RNA-seq) of flow-sorted PCs, GC (LZ and DZ populations) and naive B cells from immunized aPIK3CD and WT littermate controls. To eliminate any effects of aPIK3CD on early B cell development and to permit use of naive B cells as a

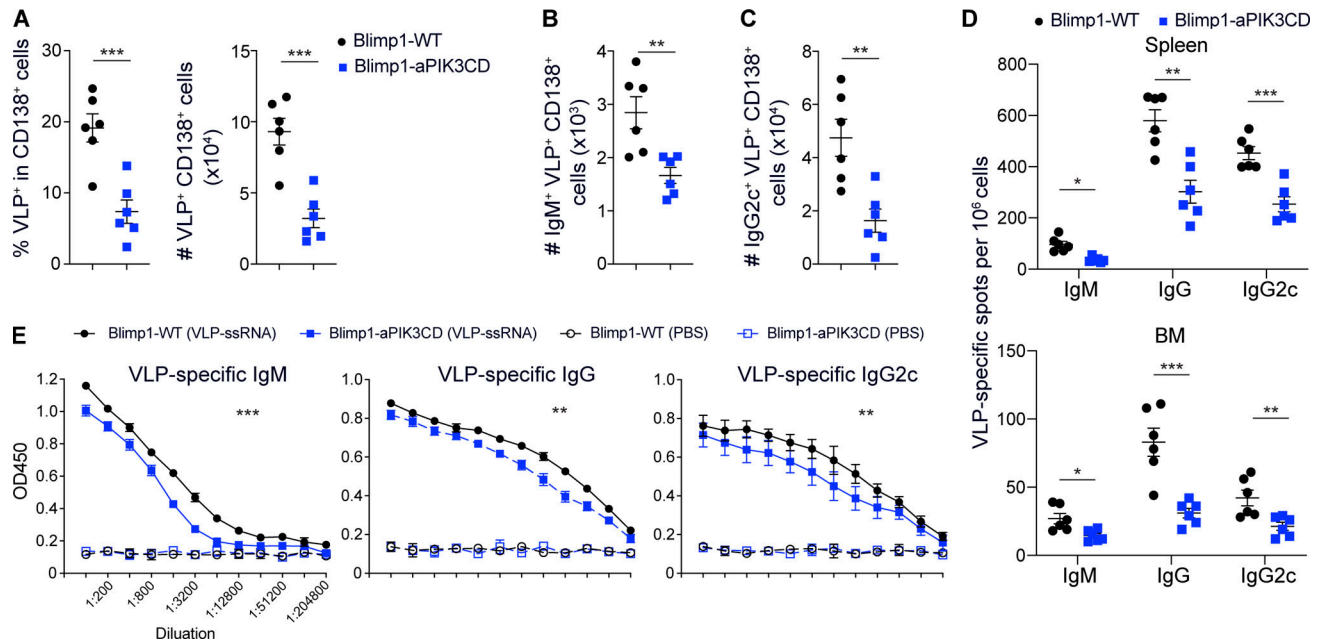


Figure 3. PC-intrinsic aPIK3CD expression alters the primary humoral response. (A) Frequency and absolute number of splenic, VLP-specific, CD138⁺ PCs in Blimp1-WT versus Blimp1-aPIK3CD mice at day 14 after immunization with VLP-ssRNA. (B and C) Quantification of IgM and IgG2c VLP-specific PCs as in A measured by flow cytometry. (D) Number of VLP-specific IgM, IgG, and IgG2c PCs in the spleen (upper) and BM (lower) determined by ELISPOT assay. (E) Dilution curves of VLP-IgM, IgG, and IgG2c from serum of immunized (filled) and unimmunized mice (open) measured by ELISA. Data are combined from two independent experiments ($n = 6$). Significance determined by unpaired Student's t test of individual groups in A–D or of area under the curve in E. *, $P < 0.05$; **, $P < 0.01$; ***, $P < 0.001$. Graphs depict mean \pm SEM.

negative control, we used AID-aPIK3CD and AID-WT mice for RNA-seq studies. Principal-component analysis showed that the GCs, naive B cells, and PCs clustered into transcriptionally distinct groups (Fig. S4 F). We did not identify differences between genotypes in naive B cells or either GC subset (adjusted $P < 0.05$; Fig. S4, G–I). However, analysis of transcriptome of PCs identified 472 differentially expressed genes (Fig. 4 A). As expected, gene set enrichment analysis

(GSEA) revealed that conventional targets of PI3K–AKT–mTORC1 signaling and mTORC1 signaling were increased in AID-aPIK3CD PCs, validating our model (Fig. 4 B). We also found that genes associated with glycolysis, protein secretion, and the UPR were increased in AID-aPIK3CD PCs. UPR genes specifically up-regulated in AID-aPIK3CD PCs included the chaperones BiP (*Hspa5*), Grp75 (*Hspa90*), and DjaJ/Hsp40 (*Dnaja3*, *Dnajb1*, and *Dnajb11*); members of the ER-associated protein degradation pathway (*Edem1* and

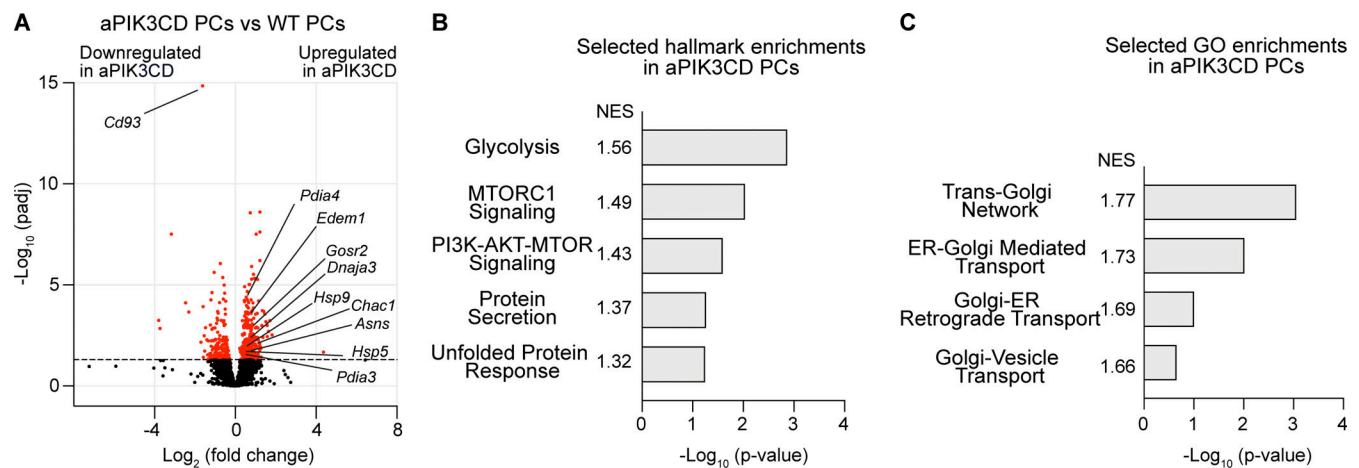


Figure 4. Altered gene expression in aPIK3CD PCs. (A) Volcano plot displays the differential gene expression of AID-aPIK3CD versus AID-WT PCs at day 14 after immunization with NP-CGG/alum. Genes in red indicate adjusted P (p_{adj}) < 0.05 . (B) Hallmark GSEA for RNA-seq data shown in a showing selected enrichments aPIK3CD PCs with normalized enrichment score (NES) and $-\log_{10}$ P value. (C) Gene ontology (GO) analysis showing selected enrichments with normalized enrichment score and $-\log_{10}$ P value. RNA-seq data represent four mice ($n = 4$) for each genotype.

Herpud1); protein disulfide isomerases (*Pdia4* and *Pdia3*); protein trafficking effectors (*Gosr2* and *Srprb*); and metabolic regulators (*Chacl*, *Asns*, and *Slc7a5*). Also, gene ontology enrichment analysis revealed that aPIK3CD PCs were enriched for ER-genesis and activation of the secretory apparatus, including protein trafficking, ER–Golgi transport, and Golgi–vesicle transport (Fig. 4 C). Altogether, these data suggest that aPIK3CD is associated with increased transcription of PC genes associated with protein secretion.

aPIK3CD PCs exhibit altered ER structure and an increased ER stress response

To directly assess the potential role for aPIK3CD in regulating transcription of ER genes in PCs, we quantified the amount of two ER-resident proteins, PDI and BiP. Consistent with the RNA-seq data, in vitro-generated CD21-aPIK3CD PCs had an increase in mRNA encoding PDI and BiP as measured by qPCR (Fig. 5 A). We also stained PCs with an ER-Tracker fluorescent dye to measure ER content. Flow cytometry analysis revealed that the intensity of ER-Tracker staining was significantly increased in CD21-aPIK3CD PCs compared with control PCs (Fig. 5 B), indicative of a higher abundance of ER proteins.

As an independent qualitative analysis of PC morphology, we used electron microscopy to determine if aPIK3CD altered ER structure or size and/or other ultrastructural features. CD21-aPIK3CD PCs displayed multiple abnormalities as compared with controls (Fig. 5 C). The cytoplasm of most aPIK3CD PCs was densely occupied with ribosomes and mitochondria, and uniformly spaced ER structures were absent or altered in comparison to control cells (Fig. 5 C). Although some CD21-aPIK3CD ASCs exhibited an organized ER structure, in contrast to controls, these cells also contained multiple large vacuole-like structures (Fig. 5 C).

Consistent with the deregulation of ER by aPIK3CD, we found enhanced ER stress in CD21-aPIK3CD PCs, as evidenced by increased spliced XBP1, total XBP1, and Blimp1, and there was no difference in ATF4 or ATF6 (Fig. 5 D). Supporting our in vitro data, ex vivo CD21-aPIK3CD VLP-specific and polyclonal PCs, but not naive or GC B cells, displayed a significantly increased ER-Tracker staining compared with controls at days 7 and 14 after immunization with VLP-ssRNA (Fig. 5 E). Together, these data demonstrate a direct control of ER homeostasis mediated by PI3K δ -dependent signaling.

aPIK3CD inhibits autophagy in differentiating ASCs

Next, we investigated whether the autophagy pathway, critical for the breakdown of excess or damaged ER (Pengo et al., 2013), was altered in aPIK3CD PCs. Because macroautophagy (hereafter autophagy) is mainly controlled by mTORC1 (Jung et al., 2010), a key downstream target of the PI3K δ pathway, we first assessed PI3K δ and mTORC1 activity in control and CD21-aPIK3CD B cell subsets by measuring phosphorylated AKT (T308) and ribosomal protein S6 (S235/236), respectively. CD21-aPIK3CD B cells and PCs displayed significant enhanced levels of pAKT and pS6 (Fig. S5 A). Since mTORC1 negatively regulates autophagy, we hypothesized that aPIK3CD suppresses autophagy in differentiating PCs. To measure autophagy, we quantified the processing of LC3 to its autophagosome membrane-bound lipid-conjugated

form (LC3-II). Immunoblot analysis of primary splenic B cells differentiated into PCs in vitro showed that CD21-aPIK3CD cells have less accumulation of LC3-II compared with controls (Fig. 5 F). Treatment with chloroquine, an inhibitor that prevents the lysosomal breakdown of autophagosomes, increased LC3-II accumulation in both CD21-aPIK3CD and CD21-WT cells but did not fully rescue the deficit in CD21-aPIK3CD cells (Fig. 5 F). These results were further validated by quantifying the formation of LC3 puncta using fluorescence microscopy. Again, aPIK3CD cells exhibited significantly less LC3⁺ autophagosome accumulation (Fig. 5 G and Fig. S5 B). Together, these data demonstrate that autophagy is inhibited in PCs with hyperactive PI3K δ signaling.

aPIK3CD impairs PC survival

PCs require UPR and autophagy to control ER stress, and dysregulation in these pathways impairs PC survival (Auner et al., 2010; Pengo et al., 2013). Our data showed that hyperactive PI3K δ signaling leads to a decrease in splenic and BM PC numbers, suggesting that altered PC survival might be the primary driver of these abnormalities. We evaluated PC apoptosis using caspase and terminal deoxynucleotidyl transferase dUTP nick end labeling (TUNEL) assays. In vitro-cultured aPIK3CD activated B cells exhibited slightly reduced caspase and TUNEL signals at day 6 after stimulation with R848 and IL-21, consistent with slightly increased survival (Fig. S5, C and D). In contrast, CD21-aPIK3CD ASCs exhibited significant increases in both caspase and TUNEL signal relative to controls (Fig. 6, A and B). Consistent with this, MCL-1 expression, an essential anti-apoptotic BCL-2 family member for PC survival (Peperzak et al., 2013), was decreased in CD21-aPIK3CD ASCs compared with controls (Fig. 6 C). Next, we assessed survival of PCs directly ex vivo after VLP-ssRNA immunization. Our data revealed that CD21-aPIK3CD VLP-specific and polyclonal PCs exhibited significant increases in caspase compared with controls, while naive and GC B cells did not (Fig. 6 D). Together, these data show that aPIK3CD promotes PC apoptosis.

mTORC1 inhibition restores aPIK3CD PC survival and ER homeostasis

We next tested whether inhibition of PI3K δ can promote improved survival of aPIK3CD PCs. To explore this, in vitro-cultured CD21-aPIK3CD and CD21-WT B cells were allowed to expand for 4 d, and then idelalisib, a selective PI3K δ inhibitor, was added to cultures for 48 h before analysis. Idelalisib decreased the intensity of ER-Tracker staining in aPIK3CD PCs to a level comparable to untreated WT (Fig. 6 E). Importantly, the defect in PC numbers derived from in vitro-differentiated CD21-aPIK3CD B cells was also fully restored by inhibiting PI3K δ (Fig. 6 F). Next, to assess whether mTORC1 regulates PC survival in the context of hyperactive PI3K δ , we performed similar in vitro experiments and treated cells with rapamycin, a potent mTORC1 inhibitor. Indeed, rapamycin reduced the intensity of ER-Tracker staining and nearly restored PC formation in in vitro-differentiated B cells isolated from CD21-aPIK3CD mice (Fig. 6, E and F). Because mTORC1 is a key regulator of multiple biological processes, we next sought to increase autophagy, independently

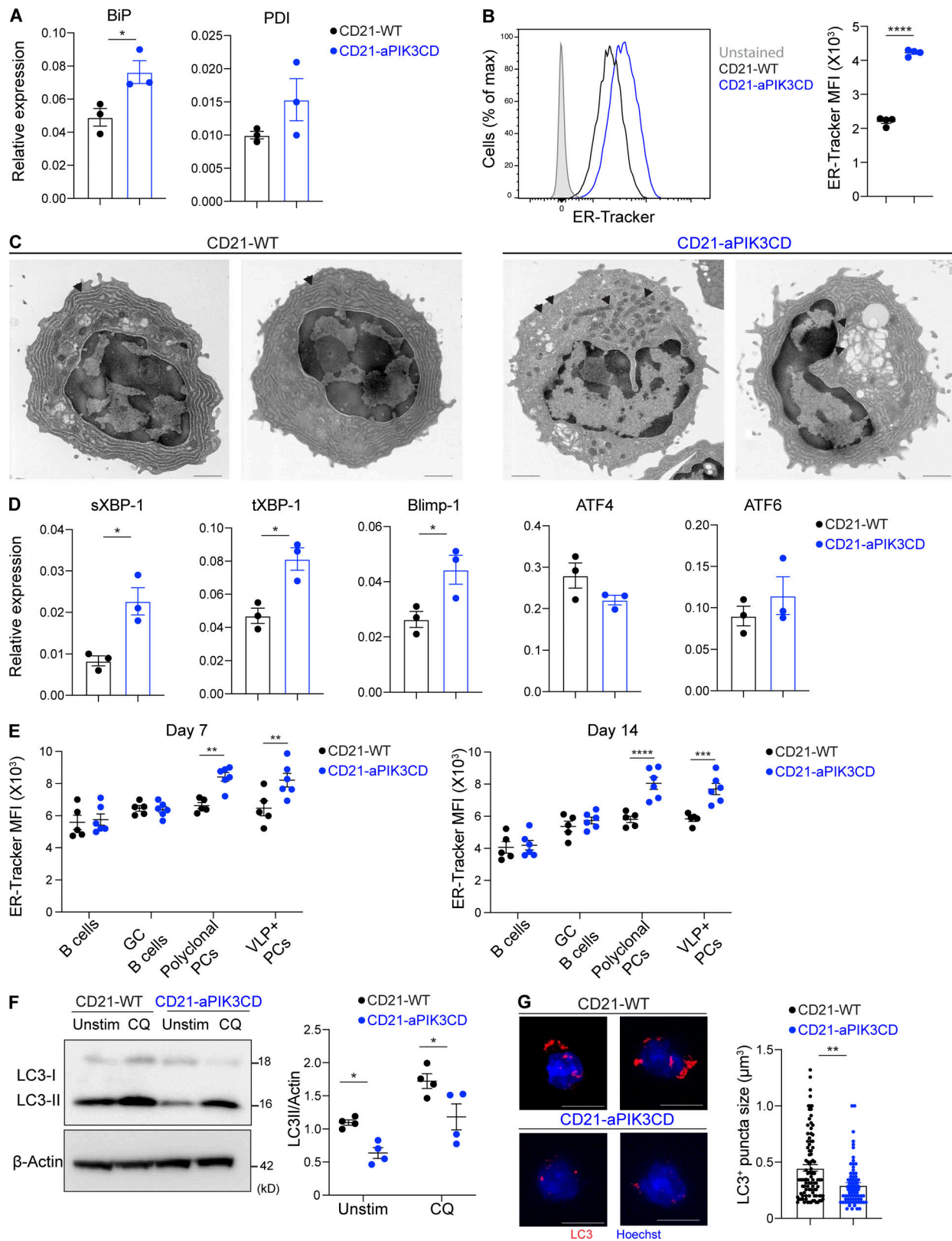


Figure 5. aPIK3CD disrupts ER homeostasis and autophagy. (A) Quantitative RT-PCR analysis of transcripts encoding BiP and PDI in CD138⁺ PCs derived from CD21-WT and CD21-aPIK3CD B cells following 6 d of in vitro culture on 40LB stroma with R848 + IL-21. mRNA expression was quantified relative to the housekeeping gene histone H3. (B) Flow cytometry analysis of ER-Tracker staining in CD138⁺ ASCs. Representative histogram overlays (left) and quantification of mean fluorescence intensities (MFI; right). (C) Representative electron microscopy images of CD21-WT and CD21-aPIK3CD ASCs sorted from in vitro cultures (scale bars = 1 μm). (D) Quantitative RT-PCR analysis of transcripts encoding spliced XBP-1 (sXBP-1), total XBP-1 (tXBP-1), Blimp-1, ATF4, and ATF6 in CD138⁺ PCs from in vitro cultures. mRNA expression was quantified relative to histone H3. (E) MFI of ER-Tracker in B220⁺ B cells, polyclonal CD138⁺ PCs, and

VLP-specific CD138⁺ PCs from CD21-WT and CD21-aPIK3CD mice at day 7 or 14 after immunization with VLP-ssRNA. **(F)** Left: Immunoblot analysis of LC3-II in CD21-WT and CD21-aPIK3CD B cells FACS-sorted after 4 d of in vitro culture and left untreated or treated with chloroquine (CQ) for 90 min. β -Actin serves as a loading control. Right: Quantification of LC3-II band intensity with or without treatment with chloroquine, presented relative to β -actin. **(G)** Left: Representative fluorescence images showing LC3⁺ puncta in CD21-WT and CD21-aPIK3CD B cells generated as in E. Right, automated quantification of LC3⁺ puncta size using ImageJ (scale bars = 5 μ m). Data are combined from two independent experiments (A and D: $n = 3$; B and F: $n = 4$; E: $n = 5-6$; G: $n = 2$). Significance determined by unpaired Student's *t* test. *, $P < 0.05$; **, $P < 0.01$; ***, $P < 0.001$; ****, $P < 0.0001$. Graphs depict mean \pm SEM.

of direct pharmacological targeting of mTORC1 using starvation (Jung et al., 2010). To assess whether induction of autophagy can contribute to PC generation, we did similar in vitro experiments, and then cultures were serum starved for 48 h before analysis. We found that starvation decreased the intensity of ER-Tracker staining and significantly increased the proportion of PCs differentiated from CD21-aPIK3CD B cells (Fig. 6 G). Together, these results demonstrate that aPIK3CD perturbs ER homeostasis and PC generation via an mTORC1-dependent signaling program.

Discussion

PIK3CD signaling exerts a critical role in immune regulation and humoral immunity (Lucas et al., 2016). Notably, the activity of PI3K δ must be precisely regulated to achieve optimal immune responses, a concept highlighted by the distinct immunodeficiency syndromes observed in human subjects with inactivating versus activating mutations in p110 δ (Fruman et al., 2017). Loss of p110 δ function leads to a severe deficit in T-independent (TI) IgM and TD IgM and IgG antibody responses (Lucas et al., 2016). In contrast, activating mutations in PIK3CD cause a human primary immune disorder characterized, in part, by enhanced TI antibody responses and conversely, reduced IgG levels and a deficit in switched and unswitched MBCs (Angulo et al., 2013; Crank et al., 2014; Lucas et al., 2014; Coulter et al., 2017). The complex and diverse phenotype observed in APDS patients, which extends beyond features described here (Coulter et al., 2017), underscores the pleiotropic effects of PI3K δ in distinct immune cell lineages. To better define the impact of activated PI3K δ signaling in specific cell types, we previously generated a conditional aPIK3CD mouse model that permits precise lineage- and developmental stage-specific modeling of aPIK3CD in an immune competent setting (Wray-Dutra et al., 2018). In this study, we investigated the specific role of elevated PI3K δ activity in the differentiation and function of MBCs and PCs. B cell-intrinsic expression of aPIK3CD led to increased formation of antigen-specific IgM and switched MBCs. Consistent with the elevated numbers of MBCs, aPIK3CD mice generated increased numbers of ASCs and more robust antibody responses following rechallenge. However, despite this initial amplified response, antibody levels declined rapidly correlating with reduced numbers of splenic and BM PCs. Our studies provide a detailed mechanistic explanation for these important and surprising observations. We demonstrate that aPIK3CD uniquely impairs PC survival by limiting autophagy and increasing ER stress, perturbations likely to be driven by the mTORC1 pathway. Our combined findings show that PI3K δ must be precisely modulated to

control ER homeostasis and permit PC generation and survival.

APDS patients exhibit a proportional and, over time, numerical reduction in unswitched and class-switched MBCs (Coulter et al., 2017; Angulo et al., 2013; Crank et al., 2014; Avery et al., 2018). However, the impact of aPIK3CD on antigen-specific MBC populations has not been explored. To address the cell-intrinsic impact of aPIK3CD in B cell memory, we assessed antigen-specific MBCs in aPIK3CD mice immunized with TD antigens. Both IgM and switched antigen-specific MBC compartments were expanded in CD21-aPIK3CD mice. These findings correlated with the impact of aPIK3CD within the GC, leading to generation of larger numbers of antigen-specific MBCs, observations corroborated by the competitive advantage of aPIK3CD versus WT antigen-specific GC B cells in BM chimeras. Further, the increase of IgM MBCs in CD21-Cre, but to a lesser extent in AID-Cre, aPIK3CD mice implies that many IgM MBCs are likely generated extrafollicularly, independent of GCs (Viant et al., 2021; Harms Pritchard et al., 2019 Preprint). These IgM MBCs may preferentially derive from activation of B cells within the expanded marginal zone compartment present in aPIK3CD mice; findings also consistent with the proportional increase of IgM versus switched MBCs in APDS subjects. Importantly, while our data showing increased MBCs in aPIK3CD mice appear distinct from the reduced number of switched MBCs in APDS patients, our current and previous observations suggest that the MBC deficit in the setting of global aPIK3CD likely reflects the combined impacts of reduced generation of naive B cells (secondary to reduced BM B lymphopoiesis), alterations in the BCR repertoire with MZ compartment skewing and a partial CSR defect. Finally, despite our new data and previous findings implying that the humoral deficits in APDS are predominantly B cell intrinsic, we cannot exclude additional B cell-extrinsic impacts caused by aPIK3CD on MBC development, particularly with respect to the functional activities of T follicular helper cells (Bier et al., 2019; Preite et al., 2018).

The expanded MBC compartment in B cell-intrinsic aPIK3CD mice correlated with greater numbers of splenic ASCs and a more robust initial antibody response following antigen rechallenge. However, splenic ASCs in aPIK3CD mice were smaller in size, and antigen-specific antibody levels rapidly declined. Further, despite the increase in splenic ASCs, BM ASC numbers did not increase, suggesting that ASC survival was reduced in aPIK3CD mice. Consistent with this concept, despite preferential expansion of antigen-specific aPIK3CD GCs and MBCs, we observed a bottleneck in the generation of antigen-specific PCs derived from aPIK3CD-expressing B cells in BM chimeras. In further support of the concept that aberrant PIK3CD signaling compromises PC formation, primary immunization in both

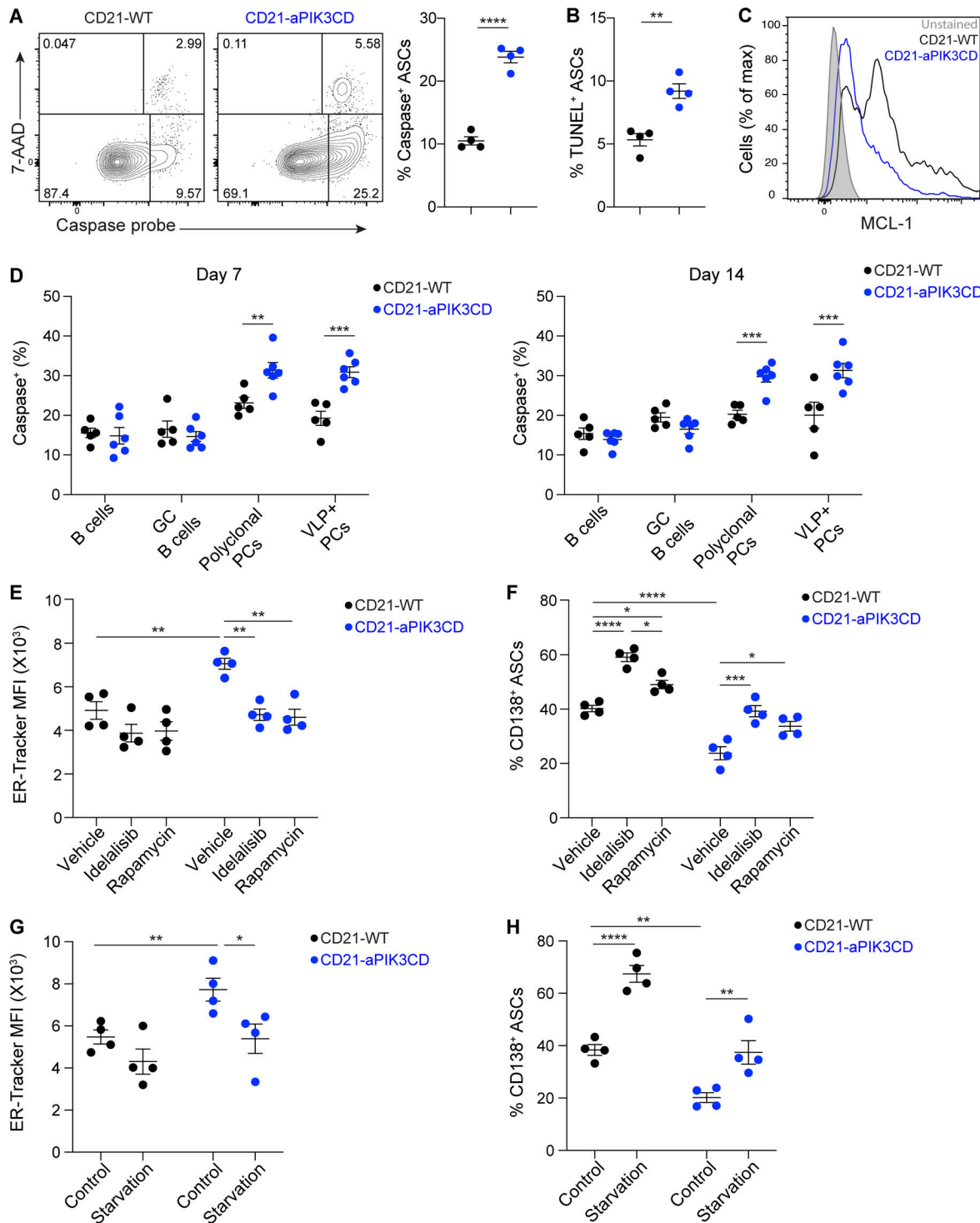


Figure 6. aPIK3CD promotes PC death. (A) Representative flow cytometry analysis (left) and frequency (right) of apoptotic (caspase⁺ 7-AAD⁻) CD138⁺ ASCs derived from CD21-WT versus CD21-aPIK3CD B cells following 6 d of in vitro culture on 40LB stroma and stimulation with R848 and IL-21. (B and C) Frequency of TUNEL⁺ apoptotic cells (B) and intracellular expression of MCL1 (C) within CD138⁺ ASC generated as in A. (D) Frequency of caspase⁺ 7-AAD⁻ apoptotic B cells, polyclonal PCs, and VLP-specific PCs from CD21-WT and CD21-aPIK3CD mice at day 7 or 14 after immunization with VLP-ssRNA. (E and F) CD21-WT and CD21-aPIK3CD B cells were cultured on 40LB stroma with R848 and IL-21. At day 4 in culture (48 h before analysis), vehicle (DMSO), idelalisib (100 nM), or rapamycin (0.5 nM) was added to the cultures. (E) MFI of ER-Tracker in CD138⁺ ASCs and (F) percentage of CD138⁺ ASCs at day 6. (G and H) CD21-WT and CD21-aPIK3CD B cells were cultured on 40LB stroma with R848 and IL-21. At day 4, cultures were serum starved for 48 h. MFI of ER-Tracker in CD138⁺ ASCs (G) and percentage of CD138⁺ ASCs (H) at day 6. Data are combined from two independent experiments (A, B, and E–H; n = 4; D: n = 5–6) or representative of two independent experiments (C). Significance determined by unpaired Student's *t* test (A and B) or multiple comparison (D–H). *, *P* < 0.05, **, *P* < 0.01; ***, *P* < 0.001; ****, *P* < 0.0001. Graphs depict mean ± SEM.

B cell- and PC-intrinsic aPIK3CD mice resulted in reduced generation of antigen-specific PCs. Using *in vitro* experiments, we confirmed that differentiated aPIK3CD ASCs manifest increased apoptosis and resulted in fewer ASCs following extended culture. Of note, a previous study in APDS subjects identified both an increase in circulating plasmablasts and increased apoptosis following *in vitro* stimulation of primary B cells (Wentink et al., 2017). In agreement with these observations, our data showed that aPIK3CD promoted increases in ASC formation yet decreases in PC survival.

Previous work demonstrated that aPIK3CD impairs the humoral response through defective CSR (Avery et al., 2018; Preite et al., 2018), correlating with reduced AID expression (Avery et al., 2018). Further, *in vitro*-stimulated transitional B cells from APDS patients failed to generate ASCs and acquire a normal PC differentiation program despite the expression of key early PC genes, including *PRDMI*, *XBPI*, and *IRF4* (Avery et al., 2018). Our new observations expand upon these collective findings, showing that expression of aPIK3CD following AID up-regulation or class-switching to IgG1 (using AID-Cre and C γ 1-Cre strains, respectively) limits class-switched antibody production. Additionally, our findings imply that these events occur independently of intact B cell expansion and selection within GCs (Wray-Dutra et al., 2018). Consistent with our findings, aPIK3CD or alternative models of enhanced PI3K signaling also induced elevated Blimp-1 expression and promoted premature ASC differentiation (Setz et al., 2018; Preite et al., 2018). Thus, while aPIK3CD does impact CSR, our combined data demonstrate that PC survival limits sustained antibody production in aPIK3CD mice and represents an additional driver for reduced IgG levels, implying that a similar mechanism is operative APDS subjects.

PCs continually produce and secrete vast amounts of antibodies (Helmreich et al., 1961). To adapt to this enormous metabolic challenge, the UPR is induced as activated B cells differentiate into PCs (Gaudette et al., 2020; Gass et al., 2002). Simultaneously, autophagy promotes degradation of unfolded proteins and damaged ER, a process that optimizes antibody secretion and sustains PC viability in mice and humans (Arnold et al., 2016; Halliley et al., 2015; Pengo et al., 2013). Based upon transcriptional, protein blotting, confocal microscopy, electron microscopy, and flow cytometry studies, we identified marked changes in aPIK3CD PCs, including reduction in autophagosome assembly, altered PC ultrastructure and ER contents, and up-regulation of the UPR. The observed defect in autophagy is one possible reason we find increased ribosome and ER quantity, and it may also lead to the accumulation of misfolded protein and accentuate the UPR program. Additionally, the PI3K δ -mTORC1 pathway regulates several aspects of cell growth and metabolic programs in activated B cells such as mitochondrial function and ROS production, which play important roles in PC differentiation, function, and survival (Jang et al., 2015; Jellusova and Rickert, 2016). Thus, it is possible that such metabolic changes in aPIK3CD B cells may contribute to ER stress and/or PC death, independently of autophagy. Collectively, these events lead to increased ER stress likely contributing to reduced PC survival.

We determined whether blocking PI3K δ -dependent signals might reverse the observed defects in aPIK3CD PCs. Treatment with the PI3K δ -specific inhibitor idelalisib, as well as with the mTORC1-specific inhibitor rapamycin, reversed the elevated ER content and promoted PC survival. The impact of rapamycin alone supports the interpretation that elevated aPIK3CD-driven mTORC1 signaling, which inhibits autophagy (Jung et al., 2010), promotes ER stress and PC death in aPIK3CD B cells. These results may seem confounding given that mTORC1 initiates the UPR before Blimp-1 (Benhamron et al., 2015; Gaudette et al., 2020) and that mTORC1 is required for PC generation (Jones et al., 2016), presumably via its role in priming B cells for antibody secretion by up-regulating UPR components (Benhamron et al., 2015). We propose that during PC development, mTORC1 is required early to promote UPR but that shortly after Blimp1 expression, mTORC1 is down-regulated to enable clearance of damaged ER via autophagy. This idea is consistent with transcriptional profiling data showing that mTORC1 is down-regulated in terminally differentiated human PCs (Garimalla et al., 2019). Collectively, these findings show that PCs exploit PIK3CD-mTORC1 to prepare for antibody secretion but that precise and dynamic tuning of this pathway is required for the survival of newly generated PCs to elicit optimal humoral immunity; however, the impact of aPIK3CD on mature PCs after LLPC generation remains to be addressed.

Inhibitors of PI3K δ (Rao et al., 2017; Chiu et al., 2017) and mTORC1 (Rae et al., 2016; Maccari et al., 2018; Lucas et al., 2014) partially reverse the immune dysregulation present in APDS patients, indicating that enhanced PI3K δ activity leads to broad alterations of immune function through skewing toward the mTORC1 pathway. Ongoing clinical trials for PI3K δ inhibitors in APDS will assess their long-term safety and efficacy. Our data support a potential role for PI3K inhibitors to boost humoral immune responses to acute vaccination even in the setting of short-term inhibitor therapy. Consistent with this idea, published work in both mouse and human cells has shown mTORC1 is required for PC generation but dispensable for survival of LLPCs (Nguyen et al., 2018; Jones et al., 2016). Additionally, maintenance of the UPR is essential for plasmablast adaptation to ER stress to prolong survival and sustain PC persistence and function (Tellier et al., 2016; Gass et al., 2002; Auner et al., 2010). Thus, our work supports utilization of PI3K δ /mTORC1 inhibitors in APDS and suggests that targeted immunization during such therapy may provide an efficient strategy to establish sustained pathogen-specific, PC mediated IgG production.

In summary, this study provides insight into the critical, balancing role for PI3K δ signals in PC biology, thereby expanding our understanding of PI3K δ signaling in humoral immunity. Most notably, we identify a previously unrecognized requirement for modulating PI3K δ activity in order to balance autophagy and the UPR, events essential to modulate ER stress and ensure PC survival. Our data also suggest that vaccination of APDS subjects in association with PI3K δ -mTORC1 inhibition may permit generation and survival of pathogen-specific LLPCs, improving immunity to infection. Conversely, enhancing PI3K δ activity may provide a means to trigger early PC death and

dampen autoantibody responses and/or potentially limit survival of PC-derived malignancies.

Materials and methods

Mice

CD21-Cre (Cr2-Cre, 006368), AID-Cre (Aicda-Cre, 007770), $\text{C}\gamma$ 1-Cre (Ighg1-Cre, 010612), Blimp1-Cre (Prdm1-Cre, 008827), R26R-EYFP (006148), B6 (C57BL/6J, 000664), and B6 CD45.1 (002014) mice were originally purchased from Jackson Laboratory and bred/maintained in specific pathogen-free facility at Seattle Children's Research Institute. $\text{Pik3cd}^{\text{E1020K/+}}$ mice were generated in our laboratory as previously described (Wray-Dutra et al., 2018). All mice were maintained on C57BL/6 background. Male and female 10- to 14-wk-old mice were used in the experiments. Animal experiments were conducted according to the protocols approved by Institutional Animal Care and Use Committee at Seattle Children's Research Institute.

Mouse immunization

Mice were injected intraperitoneally with 2 μg VLP-ssRNA, or RNA-free VLP for secondary challenge experiments, in PBS. For NP-CGG immunization, mice were intraperitoneally immunized with 100 μg NP-CGG (Biosearch Technologies) in alum (Imject Alum Adjuvant; Thermo Fisher Scientific) at 1:1 ratio. Analysis was performed after immunization at time points described in the text. All VLP reagents were provided by B. Hou (Chinese Academy of Sciences, Beijing, China).

Flow cytometry and cell sorting

Spleens and BM were harvested into ice-cold FACS buffer (PBS with 2% FBS). Cells were resuspended in RBC lysis buffer (ACK), incubated for 2–3 min, and then spun down and resuspended in FACS buffer. Samples were then filtered through 70- μm cell strainers (Corning). Single-cell suspensions were stained with fluorescence-labeled antibodies for 20–30 min at 4°C. Intracellular staining was performed using Fixation/Permeabilization (Cytofix/Cytoperm; BD Biosciences) following cell-surface staining according to the manufacturer's instructions. For Mcl-1 staining, intracellular staining was performed using the Foxp3 Staining Buffer Set (eBioscience) following cell-surface staining according to the manufacturer's instructions. For pS6 and pAKT, cells were directly fixed in 4% paraformaldehyde for 20–30 min at 4°C, followed by permeabilization cells at using cold Phosflow Perm Buffer III (BD Biosciences) for at least 30 min, then cells stained with surface and phospho-site antibodies for 35 min at 4°C.

The initial gating strategy performed included forward scatter (FSC)-A/side scatter (SSC)-A, exclusion of doublets (through SSC-H/SSC-W and FSC-H/FSC-W), and live cells. Cell counts were determined using Spherotech Accucount Fluorescent Beads (Thermo Fisher Scientific). After total cell calculation, the number of specific populations was determined by the frequency of the population determined by flow cytometry. Samples were acquired on a LSRII (BD Biosciences) flow cytometer, and data were analyzed using FlowJo software (Tree Star). For cell sorting, cells were prepared and stained as

described above and sorted on FACSaria II (BD Biosciences) flow cytometer.

Reagents

The following reagents were used according to the manufacturer's instructions: violet live caspase probe (BD Biosciences), in situ cell death detection kit, fluorescein (TUNEL; Sigma), and ER-Tracker Red (BODIPY TR Glibenclamide; 200 nM; Invitrogen). Anti-murine antibodies used in the study include the following: B220 (RA3-6B2), CD19 (1D3), CD138 (281-2), GL7 (GL7), CD38 (90), IgM (II/41), and IgD (11-26) from BioLegend; IgG2c (polyclonal) from Southern Biotech; CXCR4 (2B11), CD86 (GL1), CD73 (TY/11.8), CD80 (16-10A1), F4/80 (BM8), CD3 (145-2C11), CD45.1 (A20), CD45.2 (104), Mcl1 (D2W9E), H2kd (SF1-1.1), SA-APC-Cy7, and SA-FITC from BD Biosciences; SA-PE-AF647 from Thermo Fisher Scientific; and pS6 (Ser235/236; D57.2.2E) and pAKT (Thr308; D25E6) from Cell Signaling.

Enrichment

Splenic cell suspensions were prepared and resuspended in 200 μl FACS buffer and first incubated with 1 μg PE-AF647 (Decoy) at room temperature (RT) for 10 min. 1 μg VLP-AF647 was then added, with a final VLP-AF647 concentration \sim 2 nM, and incubated for 30 min at 4°C. Cells were washed, incubated with anti-Cy5/AF647 MicroBeads for 30 min at 4°C, and isolated with magnetic LS columns (both from Miltenyi Biotec). This enrichment method was adapted from previously described studies (Krishnamurty et al., 2016; Taylor et al., 2012; Liao et al., 2017).

BM chimeras

BM cells were isolated from leg bones (femurs and tibias) from congenically marked donors of the following genotypes: AID-Cre $\text{Pik3cd}^{\text{E1020K/+}}$ (CD45.2), AID-Cre WT (CD45.2), and AID-Cre WT (CD45.1/2). Bones were rinsed in PBS and then ground using a pestle. Extracted cells were washed in PBS, resuspended in RBC lysis buffer (ACK), and filtered through 70- μm strainers. Single-cell suspensions were resuspended in PBS and mixed at 1:1 ratio, and the ratio of cells mixed was confirmed prior injection by flow cytometry. WT (CD45.1) recipient mice were lethally irradiated (950 rads) and retro-orbitally injected with total 5×10^6 cells of the indicated genotypes into each recipient \sim 4–6 h after irradiation. Mice were placed on Baytril-medicated water (5 ml/liter) for 2 wk after irradiation. Resulting BM chimeras were bled every 4 wk after transplant to check degree of chimerism, and mice were held for 10–12 wk to allow for hematopoietic reconstitution before performing experiments.

ELISA

96-well Nunc-Immuno MaxiSorp plates (Thermo Fisher Scientific) were coated overnight at 4°C with 2 $\mu\text{g/ml}$ VLP, 35 $\mu\text{g/ml}$ NP4-BSA, or 35 $\mu\text{g/ml}$ NP30-BSA (Biosearch Technologies) in PBS. Plates were blocked with 2% BSA before sample incubation, and then plates were incubated with serially diluted serum at RT for 2 h. Subsequently, plates were incubated with HRP-conjugated goat anti-mouse IgM, IgG, IgG1, or IgG2c (1:2,000 dilution; Southern Biotech). Peroxidase reactions were developed

using OptEIA TMB substrate reagent set (BD Biosciences) and stopped with sulfuric acid. Absorbance was measured at 450 nm using a SpectraMax i3X microplate reader (Molecular Devices).

ELISPOT

MultiScreen 96-well ELISPOT plates (Millipore) were coated overnight at 4°C with 2 µg/ml VLPs. Plates were blocked with 10% FBS in complete DMEM (Thermo Fisher Scientific) for 1 h at RT. Serially diluted cells were added to the plate and then incubated overnight at 37°C in 5% CO₂. Cells were washed off, and plates were incubated with HRP-conjugated goat anti-mouse IgM, IgG, or IgG2c (1:2,000 dilution; Southern Biotech). Non-specific (background) spots were determined in wells containing no cells. Spots were developed using the AEC substrate kit (Vector Laboratories) and scanned and counted using the CTL ELISPOT reader and Immunospot analysis software (Cellular Technology).

In vitro cell culture assays

The in vitro differentiation system using 40LB stromal cells was performed as described previously (Haniuda and Kitamura, 2019; Nojima et al., 2011). In brief, 40LB cells (in complete DMEM supplemented with 10% FBS; Thermo Fisher Scientific) were inactivated by irradiation. Splenic B cells, enriched using EasyStep mouse B cell isolation kit (Stem Cell Technologies), were plated onto the 40LB cells cultured in IMDM medium (supplemented with 10% FBS and 2-mercaptoethanol; Thermo Fisher Scientific) and stimulated with recombinant IL-4 (1 ng/ml), IL-21 (10 ng/ml), R848 (1 µg/ml), and/or LPS (1 µg/ml) for 4 d. At day 4, stimulated B cells were transferred onto fresh 40LB cells and cultured in new IMDM media with indicated stimulations. For inhibitor experiments, vehicle (DMOS), idelalisib (100 nM; Selleck Chemicals), or rapamycin (0.5 nM; Selleck Chemicals) was added to the cultures 48 h before analysis. For serum starvation experiments, cultures were either received full serum (10%) or serum deprived (0%) media. Cells were analyzed by flow cytometry at indicated time points.

RNA-seq and analysis

500 cells (from four biological replicates for each genotype, where each replicate represents one mouse) were sorted directly into reaction buffer from the SMART-Seq v4 Ultra Low Input RNA Kit for Sequencing (Takara), and reverse transcription was performed, followed by PCR amplification to generate full-length amplified cDNA. Sequencing libraries were constructed using the NexteraXT DNA sample preparation kit (Illumina) to generate Illumina-compatible barcoded libraries. Libraries were pooled and quantified using a Qubit Fluorometer (Life Technologies). Dual-index, single-read sequencing of pooled libraries was performed on a HiSeq2500 sequencer (Illumina) with 58-base reads using HiSeq v4 Cluster and SBS kits (Illumina) with a target depth of 5 million reads per sample. Base calls were processed to FASTQs on BaseSpace (Illumina), and a base call quality-trimming step was applied to remove low-confidence base calls from the ends of reads. The FASTQs were aligned to the mouse reference genome using STAR v.2.4.2a and gene

counts were generated using htseq-count. Quality control and metrics analysis was performed using the Picard family of tools (v1.134).

Differential expression was analyzed for each cell type by DESeq2. Genes with an adjusted P value of < 0.05 were called as significantly differentially expressed. GSEA was performed using the GSEA software from the Broad Institute. Genes were ranked based on $-\log(\text{padj}) \times \log_2(\text{FoldChange})$ from the DESeq2 package and compared with GSEA-defined gene sets. RNA-seq datasets were deposited in the Gene Expression Omnibus (accession no. GSE171795)

Electron microscopy

CD138⁺ PCs were sorted, gently pelleted, and resuspended in 1/2 strength Karnovsky's EM fixative (2% paraformaldehyde and 2.5% glutaraldehyde in 0.1 M cacodylate buffer, pH 7.4) overnight at 4°C. Cells were rinsed by pelleting and resuspending with several changes of 0.1 M cacodylate buffer and postfixed with 1% osmium tetroxide (EMS Diasum) for 90 min at 4°C. The samples were rinsed several times with cacodylate buffer and dehydrated through a graded series of ethanols. Cell pellets were incubated in a 1:1 epon 12 resin (Ted Pella) to ethanol mixture overnight on a rotator and exchanged with two fresh resin changes the following day. A final resin change was made and allowed to polymerize overnight in a 60°C oven. 70-nm ultrathin sections were obtained with a Leica UC7 ultramicrotome, put onto 150-mesh carbon-coated grids, and stained with uranyl acetate and lead citrate. Sections were examined with an FEI TF20 transmission electron microscopy (TEM) operated at 200 kV and imaged with a high-angle annular dark-field scanning TEM (HAADF STEM) detector. Images were inverted to bright field using ImageJ.

Quantitative PCR

Total RNA was isolated from FACS-sorted PCs using RNeasy Mini Kit (QIAGEN) and converted into cDNA by reverse transcription (Maxima Reverse transcription; Thermo Fisher Scientific) according to the manufacturer's instructions. Real-time PCR was performed using a CFX96 Real-Time PCR Detection System with iTaq Universal SYBR Green Supermix (Bio-Rad). Primers used were as follows: ATF4, forward 5'-GCCTGACTCTGC TGCTTACATTAC-3', reverse 5'-CCCTTGCTTACGGACCTCTTC-3'; ATF6, forward 5'-CAGAGGCAGCACACGCATTC-3', reverse 5'-GGTCAGCAGGAGCAGAGAAGG-3'; Blimp-1, forward 5'-GTGTGG TATTGTCTGGGACTTTG-3', reverse 5'-GGACTCTTTGGGTAGA GTTC-3'; tXBPI, forward 5'-AAGAACACGCTTGGGAATGG-3', reverse 5'-ACTCCCCTTGGCCTCCAC-3'; sXBPI, forward 5'-GAGTCC GCAGCAGGTG-3', reverse 5'-GTGTCTCAGAGTCCATGGGA-3'; PDI, forward 5'-TAGCAAAGGTGGATGCCACA-3', reverse 5'-CACCAT ACTGCTGAGCCAGGT-3'; BiP, forward 5'-TATTGGAGGTGGCA AACCAAG-3', reverse 5'-CGCTGGGCATCATTGAAGTAAG-3'; histone H3, forward 5'-GTGAAGAACTCATCGTTACAGGCCCT GGT-3', reverse 5'-CTGCAAAGCACC AATAGCTGCACTCTGGAA-3'. PCR was performed with the following conditions: denaturation at 95°C for 5 min; amplification, 40 cycles at 95°C for 10 s, 60°C for 30 s, and 72°C for 30 s. All reactions were standardized to the housekeeping gene histone H3.

Confocal microscopy and image analysis

FACS-sorted B cells were seeded onto poly-L-lysine-coated glass coverslips (BD BioCoat) in complete RPMI 1640 and allowed to attach for 1 h at 37°C. After plating, cells were fixed with 4% paraformaldehyde for 20 min at RT and permeabilized with saponin (0.2% saponin in PBS, 0.03 M sucrose, and 1% BSA) for 10 min at RT. Cells were blocked to prevent nonspecific binding by incubating for 1 h at RT with blocking buffer (2% goat serum, 1% BSA, 0.1% cold fish skin gelatin, 0.1% saponin, and 0.05% Tween-20 in 0.01 M PBS, pH 7.2). Cells were incubated overnight at 4°C with primary antibody (LC3, 1:500 dilution) in dilution buffer (PBS, 0.05% Tween-20, 1% BSA, and 0.1% saponin). Cells were washed three times in dilution buffer (5 min each time), incubated in secondary antibodies (1:500 dilution) in dilution buffer for 1 h at RT, and washed three times in dilution buffer. Cell nuclei were stained with Hoechst 33342 and washed twice with PBS, and the coverslips were mounted with ProLong Glass Antifade (Invitrogen). Cells were imaged on a $\times 63$ oil objectives (aperture 1.4), and images were captured on a Leica TCS SP5 confocal microscope. Postacquisition analysis, such as contrast adjustment and z-slice stacking, were performed using FIJI software, and quantification of LC3 puncta was performed using 3D Object Counter plugin from FIJI. LC3 puncta were quantified by defining LC3-staining patterns as distributed around the nucleus and as punctate. The volume of LC3 punctate was obtained by setting 85–95 intensity threshold and 3–60 voxels unit size, and the percentage of LC3 punctate-positive cells was obtained by counting total nucleus and nucleus surrounded with LC3 puncta.

Immunoblot analysis

Sorted cells were lysed for 30 min on ice in radioimmunoprecipitation assay buffer (Thermo Fisher Scientific) supplemented with phosphatase and protease inhibitor cocktail and dithiothreitol. Lysates were centrifuged for 10 min at 4°C at 14,000 *g* and supernatant was collected. Proteins were separated by electrophoresis using NuPage-Bis-Tris gels (Invitrogen) and blotted onto polyvinylidene fluoride membranes. Nonspecific binding was blocked by 5% BSA in TBS-Tween followed by incubation with LC3 primary antibody (1:2,000 dilution) overnight at 4°C and secondary antibody HRP-conjugated antibody (1:5,000 dilution) for 1 h at RT. Membranes were thoroughly washed with TBS-Tween after antibody incubations and developed using ECL reagents (Millipore). For reprobing, blots were stripped for 10 min at RT with Restore PLUS stripping buffer (Thermo Fisher Scientific). Blots were then incubated with β -actin primary antibody (1:5,000 dilution) and secondary antibody HRP-conjugated antibody (1:5,000 dilution) for 1 h at RT, washed with TBS-Tween, and developed using ECL reagents (Cytiva Amersham). ImageJ software was used for band densitometry.

Statistical analysis

Statistical significance was determined with Prism 9 (GraphPad) software Version 8.0/9.0 using two-tailed unpaired Student's *t* test or ANOVA multiple comparison as indicated in each figure.

The *P* values were considered significant when $P < 0.05$ (*), $P < 0.01$ (**), $P < 0.001$ (***), and $P < 0.0001$ (****). No statistical methods were used to predetermine sample size.

Online supplemental material

Fig. S1 shows the gating strategy and characterization of VLP-specific MBCs in CD21-aPIK3CD and control mice. **Fig. S2** shows the GC response in CD21-aPIK3CD and control mice 14 d after VLP-ssRNA immunization. **Fig. S3** demonstrates the GC response in BM chimeras after VLP-ssRNA immunization. The figure also shows reduced PC generation *in vitro* from CD21-aPIK3CD B cells following stimulation with IL-4 + IL-21, LPS + IL-4, and LPS + IL-21. The figure also demonstrates reduced levels of NP-specific IgG1 antibodies in AID-aPIK3CD and C γ 1-aPIK3CD mice after NP-CGG immunization. **Fig. S4** shows a similar GC response in Blimp1-aPIK3CD and control mice. It also shows the gene expression analysis of naive and GC B cells sorted from AID-WT and AID-aPIK3CD mice after immunization. **Fig. S5** depicts elevated levels of pAKT and pS6 in CD21-aPIK3CD B cells and PCs. The figure also shows no impact of aPIK3CD on survival of activated B cells.

Acknowledgments

We thank V. Gersuk and the Benaroya Research Institute Genomics Core for help with RNA-seq; S. MacFarlane and P. Guo at the Fred Hutchinson Cancer Research Center Cellular Imaging Shared Resource and E. Lavoie at the University of Washington Molecular Analysis Facility for assistance with TEM and image analysis; D. Kitamura at Tokyo University of Science for kindly providing CD40L stromal cells and sharing protocol and R. Pitter for initiating and maintaining 40LB cultures in our laboratory; and S. Khim and A. Zielinska-Kwiatkowska for mouse colony maintenance.

This work was supported by the King Abdulaziz City for Science and Technology (Saudi Arabia) Graduate Scholarship Program, and the Department of Immunology, University of Washington (F. Al Qureshah) and National Institutes of Health awards DP3-DK111802 (D.J. Rawlings) and R01CA201135 (R.G. James). Additional support was provided by the Children's Guild Association Endowed Chair in Pediatric Immunology (D.J. Rawlings), the Tom Hansen Investigator in Pediatric Innovation Endowment (D.J. Rawlings), the Benaroya Family Gift Fund (D.J. Rawlings), and the Seattle Children's Research Institute, Program for Cell and Gene Therapy. EM studies were supported by the Cellular Imaging Shared Resource of the Fred Hutchinson Cancer Research Center/University of Washington Cancer Consortium (P30 CA015704).

Author contributions: F. Al Qureshah designed and performed experiments, analyzed data, generated figures, and wrote the manuscript. S. Sagadiev, S. Liu, and M. Acharya performed and analyzed immunohistochemistry and confocal microscopy experiments. C.D. Thouvenel analyzed RNA-seq data. Z.H. and B. Hou provided VLP reagents and intellectual input into experimental design and interpretation. R.G. James

and D.J. Rawlings designed and supervised the study, interpreted data, and wrote the manuscript.

Disclosures: The authors declare no competing interests exist.

Submitted: 12 May 2021

Revised: 4 August 2021

Accepted: 9 September 2021

References

- Angulo, I., O. Vadas, F. Garçon, E. Banham-Hall, V. Plagnol, T.R. Leahy, H. Baxendale, T. Coulter, J. Curtis, C. Wu, et al. 2013. Phosphoinositide 3-kinase δ gene mutation predisposes to respiratory infection and airway damage. *Science*. 342:866–871. <https://doi.org/10.1126/science.1243292>
- Arnold, J., D. Murera, F. Arbogast, J.D. Fauny, S. Muller, and F. Gros. 2016. Autophagy is dispensable for B-cell development but essential for humoral autoimmune responses. *Cell Death Differ.* 23:853–864. <https://doi.org/10.1038/cdd.2015.149>
- Auner, H.W., C. Beham-Schmid, N. Dillon, and P. Sabbattini. 2010. The life span of short-lived plasma cells is partly determined by a block on activation of apoptotic caspases acting in combination with endoplasmic reticulum stress. *Blood*. 116:3445–3455. <https://doi.org/10.1182/blood-2009-10-250423>
- Avery, D.T., A. Kane, T. Nguyen, A. Lau, A. Nguyen, H. Lenthall, K. Payne, W. Shi, H. Brigden, E. French, et al. 2018. Germline-activating mutations in *PIK3CD* compromise B cell development and function. *J. Exp. Med.* 215:2073–2095. <https://doi.org/10.1084/jem.20180010>
- Benhamron, S., S.P. Pattanayak, M. Berger, and B. Tirosh. 2015. mTOR activation promotes plasma cell differentiation and bypasses XBP-1 for immunoglobulin secretion. *Mol. Cell. Biol.* 35:153–166. <https://doi.org/10.1128/MCB.01187-14>
- Bettigole, S.E., and L.H. Glimcher. 2015. Endoplasmic reticulum stress in immunity. *Annu. Rev. Immunol.* 33:107–138. <https://doi.org/10.1146/annurev-immunol-032414-112116>
- Bier, J., G. Rao, K. Payne, H. Brigden, E. French, S.J. Pelham, A. Lau, H. Lenthall, E.S.J. Edwards, J.M. Smart, et al. 2019. Activating mutations in *PIK3CD* disrupt the differentiation and function of human and murine CD4⁺ T cells. *J. Allergy Clin. Immunol.* 144:236–253. <https://doi.org/10.1016/j.jaci.2019.01.033>
- Chiu, H., S. Mallya, P. Nguyen, A. Mai, L.V. Jackson, D.G. Winkler, J.P. DiNitto, E.E. Brophy, K. McGovern, J.L. Kutok, and D.A. Fruman. 2017. The Selective phosphoinositide-3-kinase p110 δ inhibitor IPI-3063 potently suppresses B cell survival, proliferation, and differentiation. *Front. Immunol.* 8:747. <https://doi.org/10.3389/fimmu.2017.00747>
- Coulter, T.I., A. Chandra, C.M. Bacon, J. Babar, J. Curtis, N. Screaton, J.R. Goodlad, G. Farmer, C.L. Steele, T.R. Leahy, et al. 2017. Clinical spectrum and features of activated phosphoinositide 3-kinase δ syndrome: A large patient cohort study. *J. Allergy Clin. Immunol.* 139:597–606.e4. <https://doi.org/10.1016/j.jaci.2016.06.021>
- Crank, M.C., J.K. Grossman, S. Moir, S. Pittaluga, C.M. Buckner, L. Kardava, A. Agharahami, H. Meuwissen, J. Stoddard, J. Niemela, et al. 2014. Mutations in *PIK3CD* can cause hyper IgM syndrome (HIGM) associated with increased cancer susceptibility. *J. Clin. Immunol.* 34:272–276. <https://doi.org/10.1007/s10875-014-0012-9>
- Dengler, H.S., G.V. Baracho, S.A. Omori, S. Bruckner, K.C. Arden, D.H. Castellon, R.A. DePinho, and R.C. Rickert. 2008. Distinct functions for the transcription factor Foxo1 at various stages of B cell differentiation. *Nat. Immunol.* 9:1388–1398. <https://doi.org/10.1038/ni.1667>
- Dominguez-Sola, D., J. Kung, A.B. Holmes, V.A. Wells, T. Mo, K. Basso, and R. Dalla-Favera. 2015. The FOXO1 Transcription Factor Instructs the Germinal Center Dark Zone Program. *Immunity*. 43:1064–1074. <https://doi.org/10.1016/j.immuni.2015.10.015>
- Fruman, D.A., H. Chiu, B.D. Hopkins, S. Bagrodia, L.C. Cantley, and R.T. Abraham. 2017. The PI3K Pathway in Human Disease. *Cell*. 170:605–635. <https://doi.org/10.1016/j.cell.2017.07.029>
- Garimalla, S., D.C. Nguyen, J.L. Halliley, C. Tipton, A.F. Rosenberg, C.F. Fucile, C.L. Saney, S. Kyu, D. Kaminski, Y. Qian, et al. 2019. Differential transcriptome and development of human peripheral plasma cell subsets. *JCI Insight*. 4:126732. <https://doi.org/10.1172/jci.insight.126732>
- Gass, J.N., N.M. Gifford, and J.W. Brewer. 2002. Activation of an unfolded protein response during differentiation of antibody-secreting B cells. *J. Biol. Chem.* 277:49047–49054. <https://doi.org/10.1074/jbc.M205011200>
- Gaudette, B.T., D.D. Jones, A. Bortnick, Y. Argon, and D. Allman. 2020. mTORC1 coordinates an immediate unfolded protein response-related transcriptome in activated B cells preceding antibody secretion. *Nat. Commun.* 11:723. <https://doi.org/10.1038/s41467-019-14032-1>
- Halliley, J.L., C.M. Tipton, J. Liesveld, A.F. Rosenberg, J. Darce, I.V. Gregoretti, L. Popova, D. Kaminski, C.F. Fucile, I. Albizua, et al. 2015. Long-Lived Plasma Cells Are Contained within the CD19(-)CD38(hi)CD138(+) Subset in Human Bone Marrow. *Immunity*. 43:132–145. <https://doi.org/10.1016/j.immuni.2015.06.016>
- Haniuda, K., and D. Kitamura. 2019. Induced Germinal Center B Cell Culture System. *Bio Protoc.* 9:e3163. <https://doi.org/10.21769/BioProtoc.3163>
- Harms Pritchard, G., A.T. Krishnamurthy, J. Netland, N. Arroyo, K.K. Takehara, and M. Pepper. 2019. The Development of Optimally Responsive Plasmodium-specific CD73+CD80+ IgM+ Memory B cells Requires Intrinsic BCL6 expression but not CD4+ Tfh cells. *bioRxiv*. <https://doi.org/10.1101/564351> (Preprint posted March 1, 2019)
- Helmreich, E., M. Kern, and H.N. Eisen. 1961. The secretion of antibody by isolated lymph node cells. *J. Biol. Chem.* 236:464–473. [https://doi.org/10.1016/S0021-9258\(18\)64385-6](https://doi.org/10.1016/S0021-9258(18)64385-6)
- Hou, B., P. Saudan, G. Ott, M.L. Wheeler, M. Ji, L. Kuzmich, L.M. Lee, R.L. Coffman, M.F. Bachmann, and A.L. DeFranco. 2011. Selective utilization of Toll-like receptor and MyD88 signaling in B cells for enhancement of the antiviral germinal center response. *Immunity*. 34:375–384. <https://doi.org/10.1016/j.immuni.2011.01.011>
- Jang, K.J., H. Mano, K. Aoki, T. Hayashi, A. Muto, Y. Nambu, K. Takahashi, K. Itoh, S. Taketani, S.L. Nutt, et al. 2015. Mitochondrial function provides instructive signals for activation-induced B-cell fates. *Nat. Commun.* 6:6750. <https://doi.org/10.1038/ncomms7750>
- Jellusova, J., and R.C. Rickert. 2016. The PI3K pathway in B cell metabolism. *Crit. Rev. Biochem. Mol. Biol.* 51:359–378. <https://doi.org/10.1080/10409238.2016.1215288>
- Jones, D.D., B.T. Gaudette, J.R. Wilmore, I. Chernova, A. Bortnick, B.M. Weiss, and D. Allman. 2016. mTOR has distinct functions in generating versus sustaining humoral immunity. *J. Clin. Invest.* 126:4250–4261. <https://doi.org/10.1172/JCI86504>
- Jung, C.H., S.H. Ro, J. Cao, N.M. Otto, and D.H. Kim. 2010. mTOR regulation of autophagy. *FEBS Lett.* 584:1287–1295. <https://doi.org/10.1016/j.febslet.2010.01.017>
- Krishnamurthy, A.T., C.D. Thouvenel, S. Portugal, G.J. Keitany, K.S. Kim, A. Holder, P.D. Crompton, D.J. Rawlings, and M. Pepper. 2016. Somatic Hypermutated Plasmodium-Specific IgM(+) Memory B Cells Are Rapid, Plastic, Early Responders upon Malaria Rechallenge. *Immunity*. 45:402–414. <https://doi.org/10.1016/j.immuni.2016.06.014>
- Kurosaki, T., K. Komatani, and W. Ise. 2015. Memory B cells. *Nat. Rev. Immunol.* 15:149–159. <https://doi.org/10.1038/nri3802>
- Liao, W., Z. Hua, C. Liu, L. Lin, R. Chen, and B. Hou. 2017. Characterization of T-Dependent and T-Independent B Cell Responses to a Virus-like Particle. *J. Immunol.* 198:3846–3856. <https://doi.org/10.4049/jimmunol.1601852>
- Lucas, C.L., H.S. Kuehn, F. Zhao, J.E. Niemela, E.K. Deenick, U. Palendira, D.T. Avery, L. Moens, J.L. Cannons, M. Biancalana, et al. 2014. Dominant activating germline mutations in the gene encoding the PI(3)K catalytic subunit p110 δ result in T cell senescence and human immunodeficiency. *Nat. Immunol.* 15:88–97. <https://doi.org/10.1038/ni.2771>
- Lucas, C.L., A. Chandra, S. Nejentsev, A.M. Condliffe, and K. Okkenhaug. 2016. PI3K δ and primary immunodeficiencies. *Nat. Rev. Immunol.* 16:702–714. <https://doi.org/10.1038/nri.2016.93>
- Maccari, M.E., H. Abolhassani, A. Aghamohammadi, A. Aiuti, O. Aleinikova, C. Bangs, S. Baris, F. Barzaghi, H. Baxendale, M. Buckland, et al. 2018. Disease evolution and response to rapamycin in activated phosphoinositide 3-kinase δ syndrome: The European society for immunodeficiencies-activated phosphoinositide 3-kinase δ syndrome registry. *Front. Immunol.* 9:543. <https://doi.org/10.3389/fimmu.2018.00543>
- Nguyen, D.C., S. Garimalla, H. Xiao, S. Kyu, I. Albizua, J. Galipeau, K.Y. Chiang, E.K. Waller, R. Wu, G. Gibson, et al. 2018. Factors of the bone marrow microenvironment that support human plasma cell survival and immunoglobulin secretion. *Nat. Commun.* 9:3698. <https://doi.org/10.1038/s41467-018-05853-7>
- Nojima, T., K. Haniuda, T. Moutai, M. Matsudaira, S. Mizokawa, I. Shiratori, T. Azuma, and D. Kitamura. 2011. In-vitro derived germinal centre B cells differentially generate memory B or plasma cells in vivo. *Nat. Commun.* 2:465. <https://doi.org/10.1038/ncomms1475>

- Nutt, S.L., P.D. Hodgkin, D.M. Tarlinton, and L.M. Corcoran. 2015. The generation of antibody-secreting plasma cells. *Nat. Rev. Immunol.* 15: 160–171. <https://doi.org/10.1038/nri3795>
- Okkenhaug, K., A. Bilancio, G. Farjot, H. Priddle, S. Sancho, E. Peskett, W. Pearce, S.E. Meek, A. Salpekar, M.D. Waterfield, et al. 2002. Impaired B and T cell antigen receptor signaling in p110 δ PI 3-kinase mutant mice. *Science.* 297:1031–1034.
- Omori, S.A., M.H. Cato, A. Anzelon-Mills, K.D. Puri, M. Shapiro-Shelef, K. Calame, and R.C. Rickert. 2006. Regulation of class-switch recombination and plasma cell differentiation by phosphatidylinositol 3-kinase signaling. *Immunity.* 25:545–557. <https://doi.org/10.1016/j.immuni.2006.08.015>
- Pengo, N., M. Scolari, L. Oliva, E. Milan, F. Mainoldi, A. Raimondi, C. Fagioli, A. Merlini, E. Mariani, E. Pasqualetto, et al. 2013. Plasma cells require autophagy for sustainable immunoglobulin production. *Nat. Immunol.* 14:298–305. <https://doi.org/10.1038/ni.2524>
- Peperzak, V., I. Vikström, J. Walker, S.P. Glaser, M. LePage, C.M. Coquery, L.D. Erickson, K. Fairfax, F. Mackay, A. Strasser, et al. 2013. Mcl-1 is essential for the survival of plasma cells. *Nat. Immunol.* 14:290–297. <https://doi.org/10.1038/ni.2527>
- Preite, S., J.L. Cannons, A.J. Radtke, I. Vujkovic-Cvijin, J. Gomez-Rodriguez, S. Volpi, B. Huang, J. Cheng, N. Collins, J. Reilley, et al. 2018. Hyper-activated PI3K δ promotes self and commensal reactivity at the expense of optimal humoral immunity. *Nat. Immunol.* 19:986–1000. <https://doi.org/10.1038/s41590-018-0182-3>
- Preite, S., J. Gomez-Rodriguez, J.L. Cannons, and P.L. Schwartzberg. 2019. T and B-cell signaling in activated PI3K delta syndrome: From immunodeficiency to autoimmunity. *Immunol. Rev.* 291:154–173. <https://doi.org/10.1111/imr.12790>
- Rae, W., K.A. Ramakrishnan, Y. Gao, M. Ashton-Key, R.J. Pengelly, S.V. Patel, S. Ennis, A.P. Williams, and S.N. Faust. 2016. Precision treatment with sirolimus in a case of activated phosphoinositide 3-kinase δ syndrome. *Clin. Immunol.* 171:38–40. <https://doi.org/10.1016/j.clim.2016.07.017>
- Rao, V.K., S. Webster, V.A.S.H. Dalm, A. Šedivá, P.M. van Hagen, S. Holland, S.D. Rosenzweig, A.D. Christ, B. Sloth, M. Cabanski, et al. 2017. Effective “activated PI3K δ syndrome”-targeted therapy with the PI3K δ inhibitor leniolisib. *Blood.* 130:2307–2316. <https://doi.org/10.1182/blood-2017-08-801191>
- Rolf, J., S.E. Bell, D. Kovesdi, M.L. Janas, D.R. Soond, L.M.C. Webb, S. Santinelli, T. Saunders, B. Hebeis, N. Killeen, et al. 2010. Phosphoinositide 3-kinase activity in T cells regulates the magnitude of the germinal center reaction. *J. Immunol.* 185:4042–4052. <https://doi.org/10.4049/jimmunol.1001730>
- Sander, S., V.T. Chu, T. Yasuda, A. Franklin, R. Graf, D.P. Calado, S. Li, K. Imami, M. Selbach, M. Di Virgilio, et al. 2015. PI3 Kinase and FOXO1 Transcription Factor Activity Differentially Control B Cells in the Germinal Center Light and Dark Zones. *Immunity.* 43:1075–1086. <https://doi.org/10.1016/j.immuni.2015.10.021>
- Setz, C.S., E. Hug, A. Khadour, H. Abdelrasoul, M. Bilal, E. Hobeika, and H. Jumaa. 2018. PI3K-Mediated Blimp-1 Activation Controls B Cell Selection and Homeostasis. *Cell Rep.* 24:391–405. <https://doi.org/10.1016/j.celrep.2018.06.035>
- Stark, A.K., A. Chandra, K. Chakraborty, R. Alam, V. Carbonaro, J. Clark, S. Srisankantharajah, G. Bradley, A.G. Richter, E. Banham-Hall, et al. 2018. PI3K δ hyper-activation promotes development of B cells that exacerbate *Streptococcus pneumoniae* infection in an antibody-independent manner. *Nat. Commun.* 9:3174. <https://doi.org/10.1038/s41467-018-05674-8>
- Suzuki, A., T. Kaisho, M. Ohishi, M. Tsukio-Yamaguchi, T. Tsubata, P.A. Koni, T. Sasaki, T.W. Mak, and T. Nakano. 2003. Critical roles of Pten in B cell homeostasis and immunoglobulin class switch recombination. *J. Exp. Med.* 197:657–667. <https://doi.org/10.1084/jem.20021101>
- Taylor, J.J., R.J. Martinez, P.J. Titcombe, L.O. Barsness, S.R. Thomas, N. Zhang, S.D. Katzman, M.K. Jenkins, and D.L. Mueller. 2012. Deletion and anergy of polyclonal B cells specific for ubiquitous membrane-bound self-antigen. *J. Exp. Med.* 209:2065–2077. <https://doi.org/10.1084/jem.20112272>
- Tellier, J., W. Shi, M. Minnich, Y. Liao, S. Crawford, G.K. Smyth, A. Kallies, M. Busslinger, and S.L. Nutt. 2016. Blimp-1 controls plasma cell function through the regulation of immunoglobulin secretion and the unfolded protein response. *Nat. Immunol.* 17:323–330. <https://doi.org/10.1038/ni.3348>
- Viant, C., T. Wirthmiller, M.A. ElTanbouly, S.T. Chen, M. Cipolla, V. Ramos, T.Y. Oliveira, L. Stamatatos, and M.C. Nussenzweig. 2021. Germinal center-dependent and -independent memory B cells produced throughout the immune response. *J. Exp. Med.* 218:e20202489. <https://doi.org/10.1084/jem.20202489>
- Wentink, M., V. Dalm, A.C. Lankester, P.A. van Schouwenburg, L. Schölvinck, T. Kalina, R. Zachova, A. Sediva, A. Lambeck, I. Pico-Knijnenburg, et al. 2017. Genetic defects in PI3K δ affect B-cell differentiation and maturation leading to hypogammaglobulinemia and recurrent infections. *Clin. Immunol.* 176:77–86. <https://doi.org/10.1016/j.clim.2017.01.004>
- Wray-Dutra, M.N., F. Al Qureshah, G. Metzler, M. Oukka, R.G. James, and D.J. Rawlings. 2018. Activated PIK3CD drives innate B cell expansion yet limits B cell-intrinsic immune responses. *J. Exp. Med.* 215:2485–2496. <https://doi.org/10.1084/jem.20180617>

Supplemental material

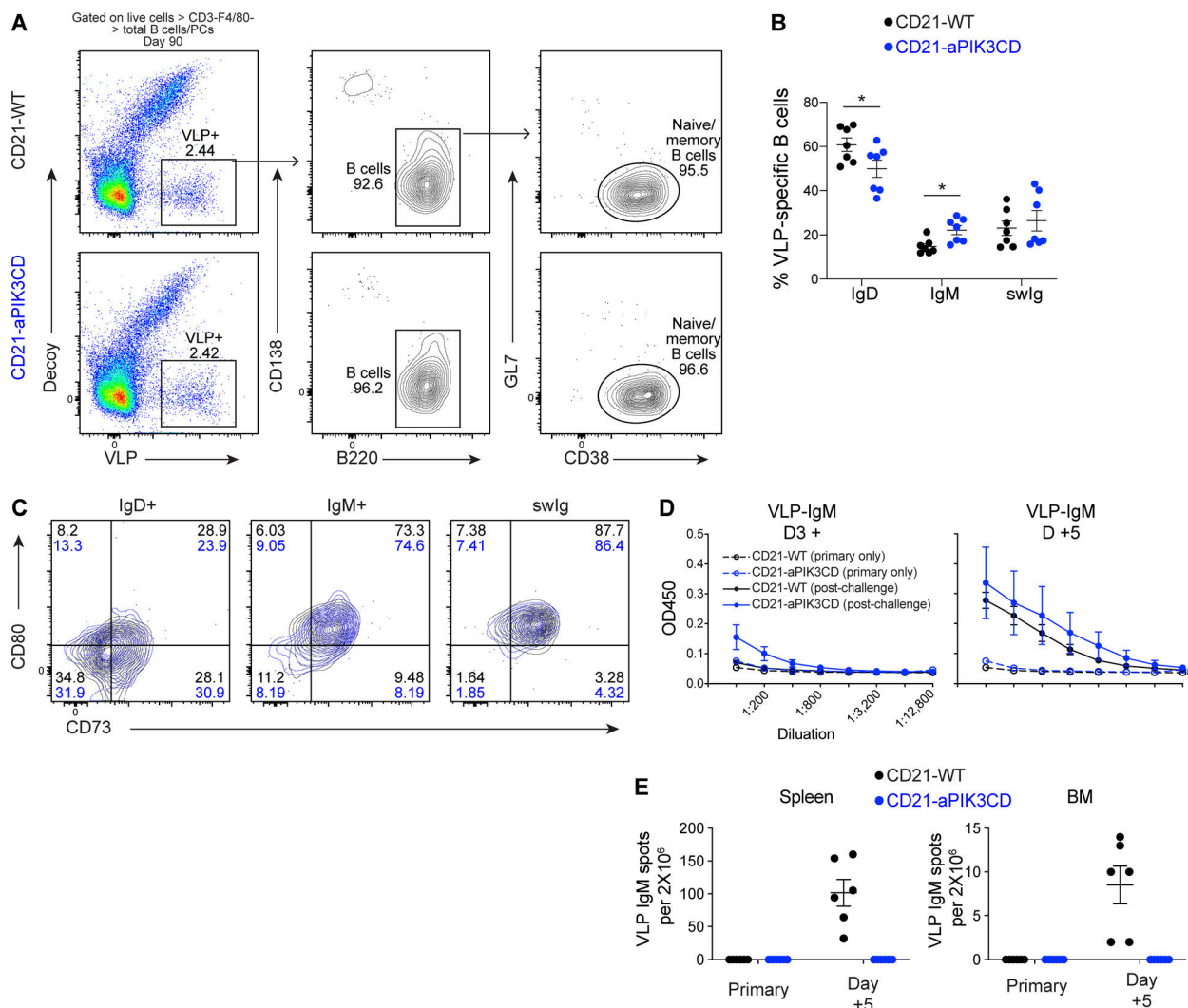


Figure S1. **Characterization of development and function of MBCs in CD21-aPIK3CD mice.** (A–C) Splenocytes from CD21-WT and CD21-aPIK3CD mice were stained first with a decoy reagent (PE-AF647) to exclude cells binding to the AF647 before adding VLP-AF647. Anti-AF647 magnetic beads were used to enrich both decoy-specific and VLP-specific B cells. (A) Gating strategy to identify VLP-specific MBCs at day 90 after immunization with VLP-ssRNA in CD21-WT versus CD21-aPIK3CD mice. Total live B220⁺ and CD138⁺ splenic B cells identified after excluding CD3⁺F4/80⁺ non-B cells and enrichment with VLP-Af647 and decoy (PE-Af647; left panels). VLP-specific B cells were identified as B220⁺CD138⁻ (middle panels). Memory/naive B cells were identified as CD38⁺GL7⁻. (B) Frequency of VLP-specific IgM, IgD, and switched MBCs at day 90 after immunization. (C) Flow cytometry analysis of CD73 and CD80 on VLP-specific IgD, IgM, and switched MBCs. (D) Dilution curves of anti-VLP-IgM in sera of mice primary-only mice or mice at days 3 or 5 after challenge as measured by ELISA. (E) Number of VLP-specific IgM spots per 2 × 10⁶ cells from the spleen (left) and BM (right) in primary-only mice or mice at 5 d after challenge. Data are combined from two (B: n = 7; D and E: n = 6) independent experiments. Significance determined by two-way ANOVA multiple comparison. *, P < 0.05. Graphs depict mean ± SEM.

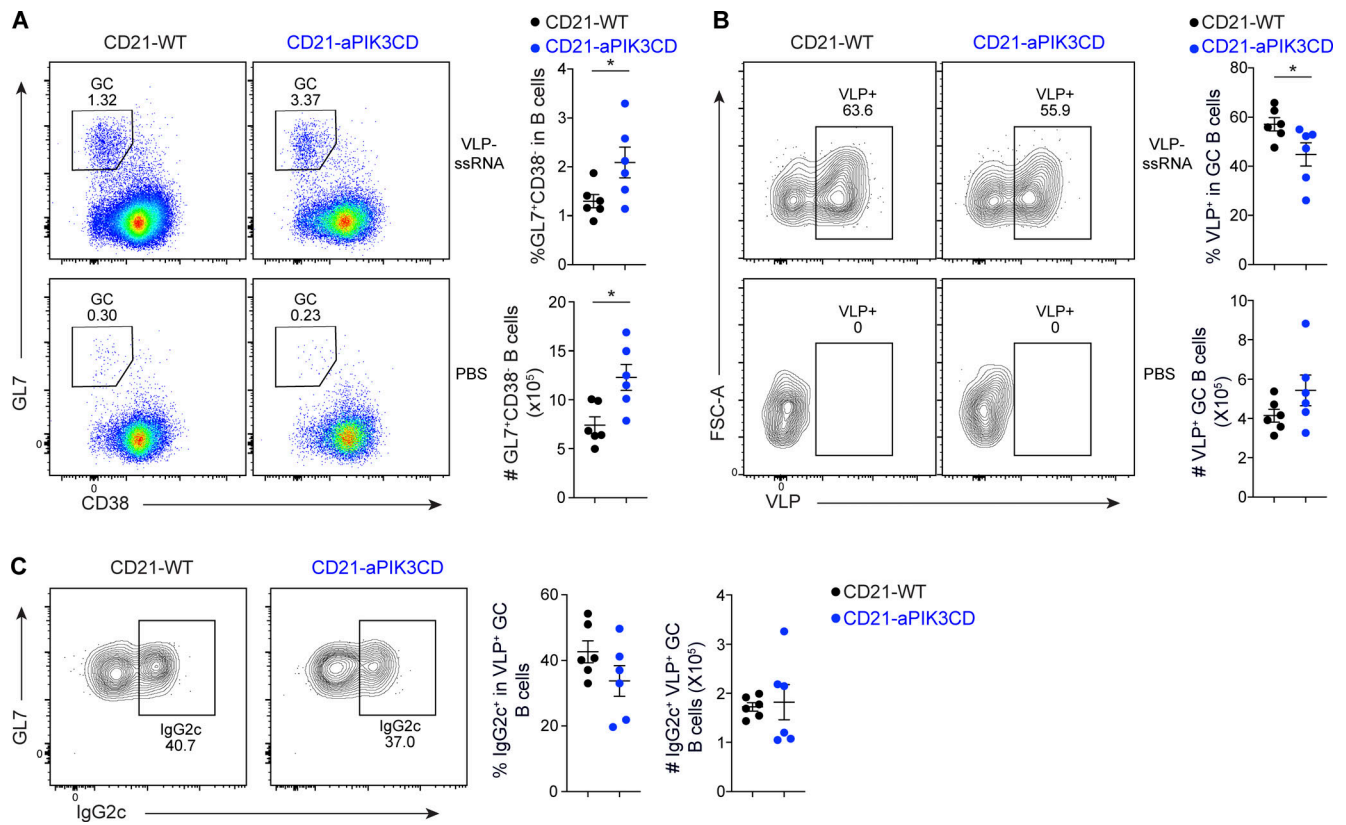


Figure S2. **GC response in B cell-intrinsic aPIK3CD model.** **(A)** Left plots show representative flow cytometry analysis of GL7⁺CD38⁻ GC B cells (initially gated on B220⁺ cells) in the spleen of 12- to 14-wk-old CD21-WT and CD21-aPIK3CD mice at day 14 d after intraperitoneal immunization with VLP-ssRNA. Right graphs show frequency and absolute numbers of GC B cells. **(B)** Left plots show representative flow cytometry analysis of VLP-specific B cells within GC in mice as described in A. Right graphs show the frequency and absolute numbers of VLP GC B cells. **(C)** Left plots show representative flow cytometry analysis of IgG2c⁺ VLP⁺ GC B cells. Right graphs show the frequency and absolute numbers of IgG2c⁺ VLP⁺ GC B cells. Data are combined from two independent experiments (*n* = 6). Significance determined by unpaired Student's *t* test. *, *P* < 0.05. Graphs depict mean ± SEM.

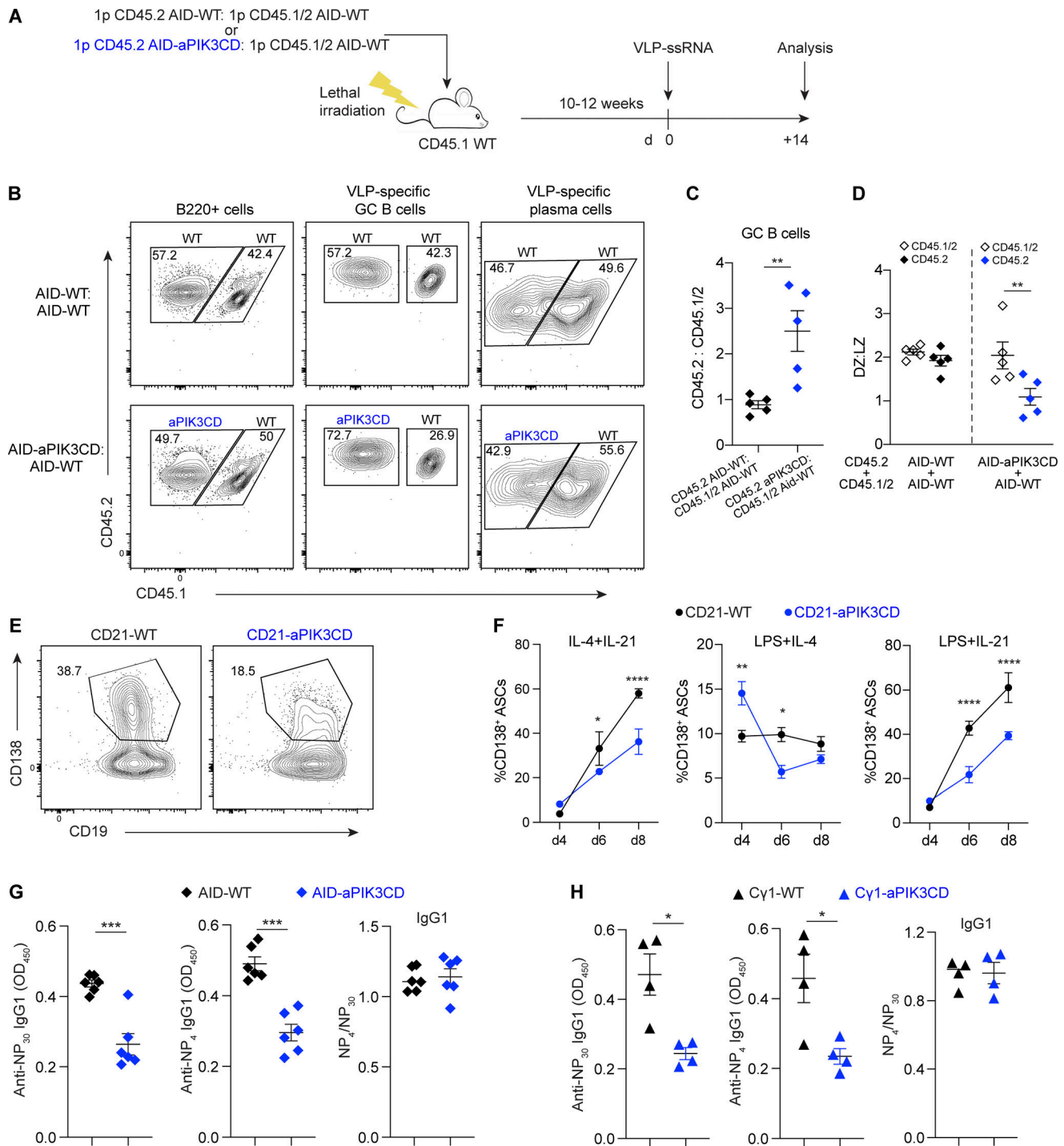


Figure S3. TD humoral response in BM chimera and different B cell-intrinsic models. (A) Schematic of the BM chimera experiments. A 1:1 ratio mixture of CD45.2 AID-WT and CD45.1/2 AID-WT or CD45.2 AID-aPIK3CD and CD45.1/2 AID-WT BM cells, respectively, were transferred to irradiated CD45.1 WT hosts. 12 wk after hematopoietic reconstitution, chimeras were immunized with VLP-ssRNA and analyzed 14 d after immunization. (B) Flow cytometry analysis of CD45.2 and CD45.1/2 staining within total B cells (left), VLP-specific GL7⁺CD38⁻ GC B cells (middle), and VLP-specific CD138⁺ PCs (right). (C) Ratio of CD45.2 to CD45.1/2 VLP-specific GC B cells in BM chimeras. (D) Ratio of DZ (CXCR4⁺CD86⁻) to LZ (CXCR4⁺CD86⁺) within GC in BM chimeras. (E) Flow cytometry analysis of CD138⁺ ASCs derived from CD21-WT versus CD21-aPIK3CD B cells cultured on 40LB stroma and stimulated with R848 and IL-21 for 6 d. (F) Percentage of CD138⁺ ASCs at days 4, 6, and 8 following cultures of CD21-WT versus CD21-aPIK3CD B cells on 40LB stroma and stimulated with IL-4 for 4 d followed by addition of IL-21 for 2 or 4 d (left), stimulated with LPS + IL-21 (middle), or stimulated with LPS + IL-21 (right). (G and H) AID-WT or AID-aPIK3CD mice or C γ 1-WT and C γ 1-aPIK3CD were immunized with NP-CGG in alum and serum collected at day 14 after immunization. (G) Total (NP₃₀; left) and high-affinity (NP₄; middle) NP-specific IgG1 measured by ELISA in AID-WT and AID-aPIK3CD mice. Right: Ratio of high-affinity to total NP-specific IgG1 (NP₄:NP₃₀). (H) Total (NP₃₀; left) and high-affinity (NP₄; middle) NP-specific IgG1 in C γ 1-WT versus C γ 1-aPIK3CD mice. Right: Ratio of high-affinity to total NP-specific IgG1 (NP₄:NP₃₀). Data are combined from two independent experiments (C and D: *n* = 5; F: *n* = 3; G: *n* = 6; H: *n* = 4). Significance determined by unpaired Student's *t* test. *, *P* < 0.05; **, *P* < 0.01; ***, *P* < 0.001; ****, *P* < 0.0001. Graphs depict mean \pm SEM.

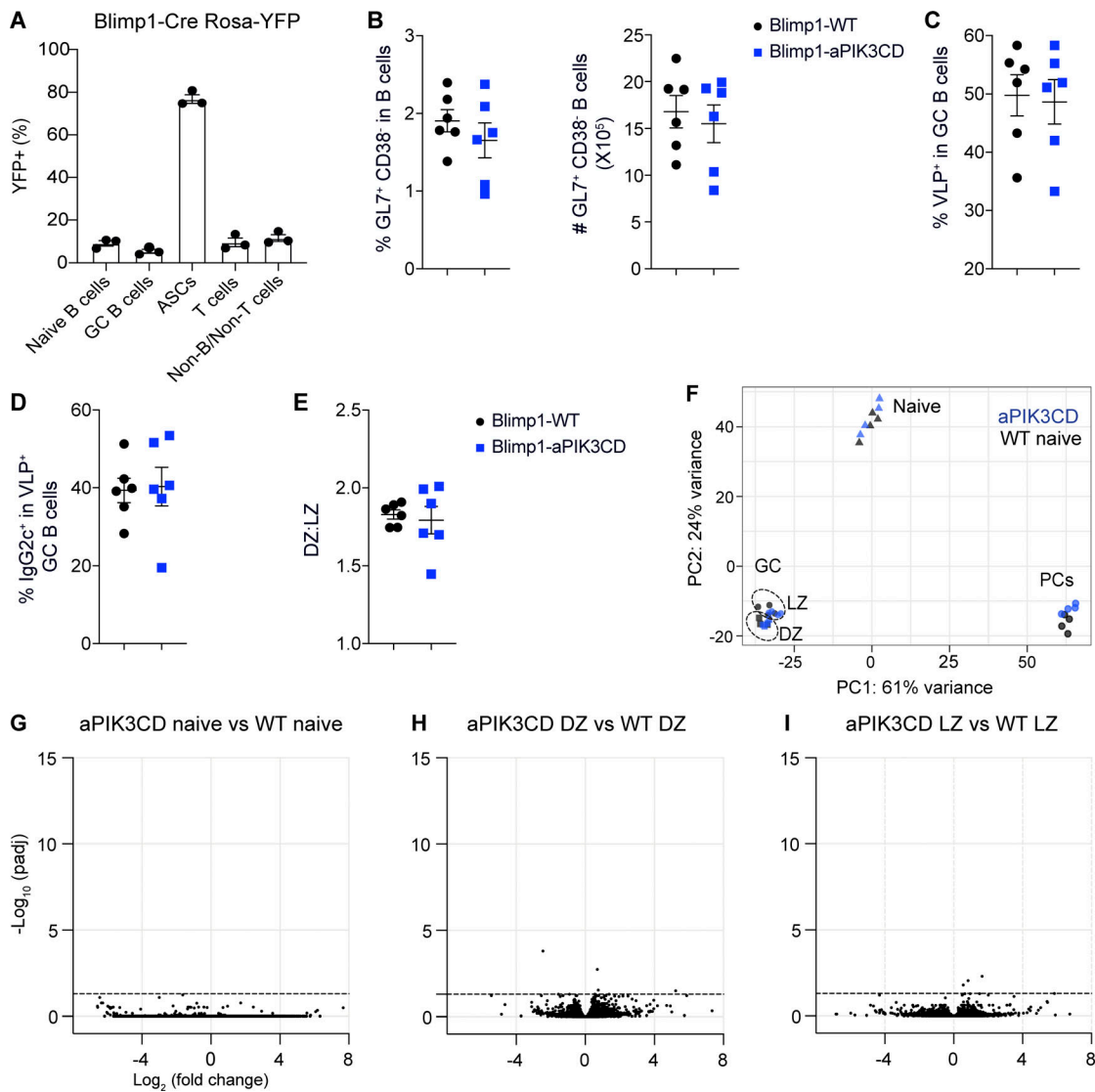


Figure S4. GC response in PC-intrinsic aPIK3CD model and gene expression analysis in naive and GC B cells. (A) Frequency of YFP⁺ cells within splenic naive B cells (B220⁺CD19⁺GL7⁻CD38⁺CD138⁻), GC B cells (B220⁺CD19⁺GL7⁺CD38⁻CD138⁻), PCs (CD138⁺), T cells (CD3⁺), and non-B/non-T cells (B220⁻CD19⁻CD3⁻CD138⁻) in Blimp1-Cre Rosa-stop-flox-EYFP mice, immunized with VLP-ssRNA and analyzed at day 14 after immunization. (B) Frequency and absolute numbers of splenic GL7⁺CD38⁻ GC B cells (among B220⁺ cells) in Blimp1Cre-WT versus Blimp1Cre-aPIK3CD mice analyzed at day 14 after immunization. (C) Frequency of VLP-specific GC B cells. (D) Frequency of IgG2c⁺ VLP-specific GC B cells. (E) Ratio of DZ (CXCR4⁺CD86⁻) to LZ (CXCR4⁺CD86⁺) within GC in mice of the indicated genotype. (F) Principal-component (PC) analysis of the RNA-seq gene expression profile of naive B cells, DZ and LZ GC B cells, and PC populations sorted from AID-WT and AID-aPIK3CD mice 14 d after immunization with NP-CGG/alum. (G-I) Volcano plots representing differential expression analysis for genes in naive B cells (G), DZ B cells (H), and LZ B cells (I). RNA-seq data (A-D) were obtained from four mice ($n = 4$) for each genotype; each symbol represents an individual mouse in A. Data are combined from two independent experiments (A: $n = 3$; B-E: $n = 6$). Graphs depict mean \pm SEM.

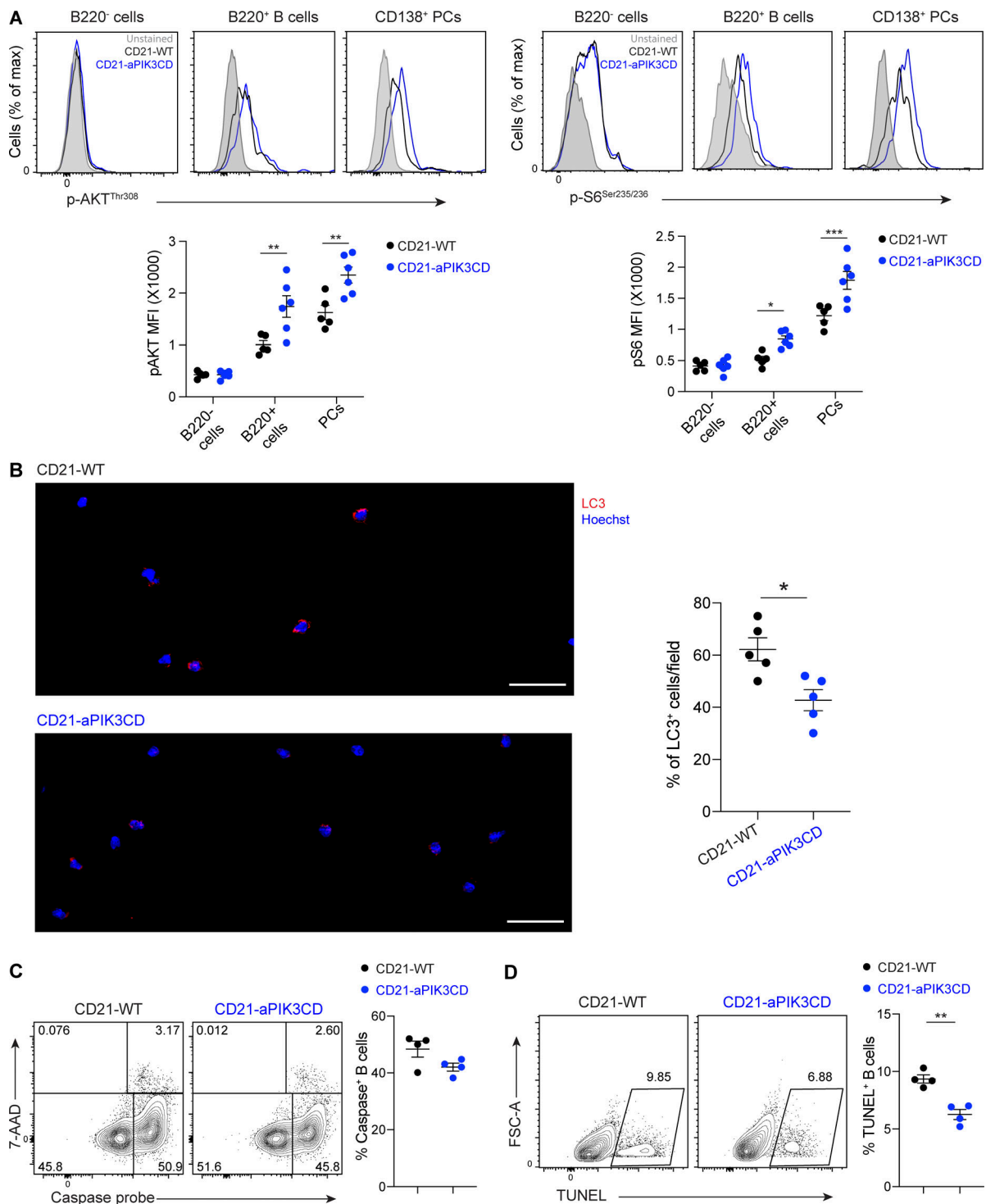


Figure S5. **Impact of aPIK3CD on autophagy and survival of activated B cells.** (A) Intracellular staining of phosphorylated Akt (T308, left) and S6 (S235/236, right) in non-B cells, B cells, and total CD138⁺ PCs from CD21-WT and CD21-aPIK3CD mice at day 14 after immunization with VLP-ssRNA. Representative histogram overlays (top) and quantification of MFI (bottom). (B) Left: Representative images of LC3 (red) and Hoechst (blue) staining of FACS-sorted CD21-aPIK3CD or CD21-WT B cells following 4 d of in vitro culture on 40LB stroma and stimulation with R848 and IL-21 (scale bars = 25 μ m). Right: Quantification of LC3⁺ cells per field. (C) Representative flow cytometry analysis (left) and frequency (right) of apoptotic (caspase⁺ 7-AAD⁻) activated B cells (CD19⁺CD138⁻) derived from CD21-WT versus CD21-aPIK3CD B cells following 6 d of in vitro culture on 40LB stroma and stimulation with R848 and IL-21. (D) Representative flow cytometry (left) and frequency (right) of TUNEL⁺ activated B cells (CD19⁺CD138⁻) cells generated as in C. Data are combined from two independent experiments (B–D: *n* = 4). Significance determined by unpaired Student's *t* test (B–D). *, *P* < 0.05; **, *P* < 0.01; ***, *P* < 0.001. Graphs depict mean \pm SEM.